STATISTICS, OPTIMIZATION AND INFORMATION COMPUTING
Stat., Optim. Inf. Comput., Vol. **x**, Month 202x, pp 1–32.
Published online in International Academic Press (www.IAPress.org)

A Fractional $SEIAQR$ Model under Caputo and Atangana–Baleanu Operators: Dynamics, Sensitivity, and Estimation for the 2024 Algeria Diphtheria Outbreak

Mohammed Amin Hakmi [1,2,*], Mohamed Nour [3]

[1] *Department of Mathematics, Institute of Science, University Center Nour Bachir, El-Bayadh, 32000, Algeria*
[2] *University of Bejaia, Faculty of Exact Sciences, LaMOS Research Unit (Modeling and Optimization of Systems), 06000 Bejaia, Algeria*
[3] *Department of Electrical Engineering, Institute of Science and Technology, University Center Nour Bachir, El-Bayadh, 32000, Algeria*

Abstract Algeria recorded a marked diphtheria resurgence in 2024, with 1124 notified cases concentrated in the southern border wilayas. We analyse a six-compartment susceptible–exposed–symptomatic–asymptomatic–quarantined–recovered ($SEIAQR$) model under two non-local operators, the singular power-law Caputo kernel and the non-singular Mittag–Leffler Atangana–Baleanu–Caputo kernel, in order to quantify how epidemic memory shapes such an outbreak. For both operators we establish positive invariance, ultimate boundedness in a compact region bounded away from extinction, and well-posedness by the Banach fixed-point theorem. The basic reproduction number is obtained in closed form and shown to be independent of the memory order; the disease-free equilibrium is locally and globally asymptotically stable for $\mathcal{R}_0 \leq 1$, and the endemic equilibrium is globally stable for $\mathcal{R}_0 > 1$ under an explicit Goh–Volterra condition. Closed-form normalized sensitivity indices identify the contact rate and the symptomatic recovery rate as the dominant levers. Calibrating a time-varying importation pulse against the 2024 INSP monthly series lowers the RMSE by about 30% and yields an endogenous $\mathcal{R}_0 \approx 0.93 < 1$: local transmission is sub-critical and the outbreak importation-sustained. A fractional optimal-control problem with three interventions cuts the infected burden by about 75%.

Keywords Fractional-order epidemiology; Caputo derivative; Atangana–Baleanu derivative; Diphtheria outbreak; Fractional optimal control

AMS 2010 subject classifications 34A08, 92D30, 93B35, 90C30, 26A33, 34D23, 49K15

DOI: 10.19139/soic-2310-5070-4585

1. Introduction

Classical compartmental models, since Kermack and McKendrick [1], are systems of first-order ordinary differential equations and therefore assume that each population class changes according to its *instantaneous* state only. Real transmission is shaped by latency, waning immunity, behavioural inertia and heterogeneous contact histories, so the present force of infection is a functional of the past. Fractional-order operators encode this *memory* through a non-local kernel and have become a standard modelling device in epidemiology [2, 3, 4].

Two operators dominate. The Caputo derivative

$$^{C}D_{0,t}^{\alpha} f(t) = \frac{1}{\Gamma(1-\alpha)} \int_0^t (t-\tau)^{-\alpha} f'(\tau)\, \mathrm{d}\tau,\ (0 < \alpha \leq 1)$$

uses a *singular* power-law kernel with algebraically decaying memory [5, 6]. The Atangana–Baleanu derivative in the Caputo sense (ABC) [7] replaces the singular kernel by the *non-singular* Mittag–Leffler kernel, which captures

*Correspondence to: Mohammed Amin Hakmi (Email: mohamedamin.hakmi@univ-bejaia.dz), University Center Nour Bachir, El-Bayadh, 32000, Algeria.

ISSN 2310-5070 (online) ISSN 2311-004X (print)

crossover between short-time exponential and long-time power-law regimes; a related non-singular construction is the Caputo–Fabrizio operator [8, 9]. The price of the ABC kernel is a more delicate numerical treatment, for which the Toufik–Atangana product scheme [10] is the reference method.

The choice of a fractional operator is not a formal generalisation; for a disease such as diphtheria it is a modelling statement about three specific mechanisms. First, *latency is not exponentially distributed*. The integer-order transfer σE from the exposed to the infectious class implicitly asserts a memoryless waiting time, so that a fixed proportion of exposed individuals progresses per unit time regardless of how long they have been exposed. Diphtheria has a well-documented incubation period of two to five days with low dispersion, and the resulting waiting-time distribution has a heavier tail and a lower early hazard than the exponential. A Caputo derivative of order $\alpha < 1$ reproduces exactly this feature: the corresponding sojourn distribution has the Mittag–Leffler survival $E_\alpha(-\sigma t^\alpha)$, whose hazard decreases with the time already spent in the class. Second, *immunity wanes and behaviour is inertial*. Diphtheria immunity conferred by DTP vaccination declines over years, and population contact behaviour responds to an outbreak with a delay and then relaxes only slowly; both effects make the current force of infection a functional of the whole epidemic history rather than of the instantaneous state. Third, *transmission in a sparse, mobile population is sub-diffusive*. In the southern Algerian wilayas the at-risk population is scattered across large distances and connected by intermittent movement, so the spatial spread of infection is slower than the linear-in-time growth implied by well-mixed mass action; anomalous, sub-diffusive transport is precisely the regime that fractional kernels encode.

These three mechanisms motivate memory, but they do not by themselves select a kernel, and the two operators used here make materially different assumptions about how memory fades. The Caputo kernel $(t-\tau)^{-\alpha}$ is singular at $\tau = t$ and decays algebraically, so that the influence of the remote past persists indefinitely, decaying like $t^{-\alpha}$; solutions of the linear problem relax as $E_\alpha(-ct^\alpha) \sim (ct^\alpha\Gamma(1-\alpha))^{-1}$, which is a power law, not an exponential. This is the appropriate description of persistent, long-range memory such as slowly waning population immunity. The Atangana–Baleanu–Caputo kernel $E_\alpha\big(-\frac{\alpha}{1-\alpha}(t-\tau)^\alpha\big)$ is bounded at $\tau = t$, and the operator carries an explicit local weight $(1-\alpha)/B(\alpha)$ on the instantaneous flux. It therefore describes a *crossover*: memory is close to exponential at short times and becomes power-law only at long times. For a disease with a short clinical course and short-to-medium-range immunity this is arguably the more realistic description, and the crossover is what makes the ABC trajectories relax measurably faster than their Caputo counterparts at the same order (Section 8). Since neither choice is dictated by the data, we instantiate the same compartmental structure under both operators and let the comparison be quantitative rather than rhetorical.

Fractional models have been applied across infectious diseases, including tuberculosis [11], COVID-19 [12], and classical epidemic and predator–prey systems [13]. Recent contributions in *Statistics, Optimization & Information Computing* illustrate the analysis–sensitivity–optimisation pipeline within which the present paper sits. Tafrikan *et al.* [14] developed a Caputo model of diphtheria spread, computed $\mathcal{R}_0$ by the next-generation matrix, and carried out a forward sensitivity analysis; it is the closest study to ours and motivates both our disease application and several modelling choices. Afiyah *et al.* [15] analysed a fractional harvested predator–prey system; Herdicho *et al.* [16] combined a hybrid Euler discretisation with Pontryagin's principle for a fractional dengue model with optimal control; Hidayat *et al.* [17] formulated a fractional monkeypox model with optimal control calibrated to real surveillance data, which is the closest methodological analogue to the estimation-then-control pipeline of Sections 7 and 9, and the same group [18] estimated the parameters of a delayed monkeypox model by least squares on reported case counts; and Alfiniyah *et al.* [19] studied optimal control of Lassa fever.

Diphtheria is a timely application. Although controlled by DTP vaccination, it retains two features that our compartmental structure represents: *asymptomatic toxigenic carriers*, who sustain transmission without symptoms (our A class), and *isolation of cases and contacts* as the principal non-pharmaceutical control (our Q class). Algeria experienced a marked resurgence in the southern wilayas over 2022–2024. According to the national surveillance bulletin of the Institut National de Santé Publique (INSP) [20], notified cases rose from 16 (2022) to 251 (2023) and 1124 (2024), the 2024 wave being concentrated in Tamanrasset and In Guezzam and epidemiologically linked to cross-border movement. We use the 2024 monthly INSP series to calibrate the model. (These national "all notified" counts exceed the WHO confirmed-only figures [21]; see Section 7.)

Three gaps in this literature motivate the present study. *(i) Kernel comparisons are qualitative.* Papers that present both a singular and a non-singular operator almost always compare them on a single figure and conclude, without measurement, that one kernel “retains less memory”; we are not aware of a fractional epidemic study that reports a quantitative, compartment-wise discrepancy metric between the two operators calibrated on the same real series. *(ii) Sub-critical outbreaks are treated as anomalies.* The standard fractional epidemic pipeline computes $\mathcal{R}_0$ and interprets $\mathcal{R}_0 < 1$ as extinction; but an outbreak that is genuinely importation-sustained has $\mathcal{R}_0 < 1$ *and* hundreds of cases, and reconciling the two requires an explicit exogenous term rather than an inflated transmission rate. *(iii) Fractional optimal control is rarely posed for such a regime.* Control analyses are almost invariably run on self-propagating outbreaks with $\mathcal{R}_0 > 1$, leaving open whether intervention is worthwhile when local transmission is already sub-critical. Accordingly, the contributions of this paper are the following.

- **A like-for-like comparison of a singular and a non-singular kernel on real epidemic data, made quantitative.** A single $SEIAQR$ structure is instantiated under both the Caputo and the ABC operators, with complete proofs of positivity, ultimate boundedness and well-posedness for each (Sections 3–4), and the two trajectory families are compared by a normalized L^1 discrepancy computed compartment by compartment (Section 8).
- **An importation pulse that explains an outbreak with endogenous $\mathcal{R}_0 < 1$.** A non-autonomous term $\iota(t)$ injects externally acquired infection into the infected classes. Calibrated against the 2024 INSP monthly series it lowers the RMSE by about 30% relative to the autonomous model and returns $\mathcal{R}_0 \approx 0.93 < 1$, showing that the 2024 Algerian wave was sustained by cross-border importation rather than by local self-propagation (Sections 7–8) — a conclusion with direct public-health consequences, since it makes border surveillance rather than general contact reduction the binding intervention.
- **Complete qualitative dynamics for both operators.** A closed-form $\mathcal{R}_0$ shown to be independent of the memory order, local stability of the disease-free equilibrium by Matignon’s criterion with the Routh–Hurwitz conditions, global stability of the disease-free equilibrium by a Goh-type linear Lyapunov functional with the fractional LaSalle principle, existence and global stability of the endemic equilibrium under an explicit Goh–Volterra condition, and closed-form normalized sensitivity indices with 95% confidence intervals (Sections 5–6).
- **Fractional optimal control of a sub-critical, importation-driven outbreak.** Three interventions — contact reduction, active isolation and enhanced treatment — are introduced with dimensionally consistent gains; existence of an optimal control is proved through the Fleming–Rishel conditions, the Caputo adjoint system and the Pontryagin characterisation are derived, and a forward–backward sweep shows that coordinated control still cuts the infected burden by about 75% even though endogenous transmission is already sub-critical (Section 9).

Throughout, $\Gamma(\cdot)$ is the gamma function and $E_\alpha(\cdot)$ the one-parameter Mittag–Leffler function.

2. Preliminaries

We assume that $\alpha \in (0, 1]$ and $f \in C^1([0, T]; \mathbb{R})$ unless stated otherwise.

Assumption 2.1 (Standing hypotheses)
Unless stated otherwise the following hold throughout the paper. The memory order satisfies $\alpha \in (0, 1]$. All demographic and epidemiological parameters $\Lambda, \mu, \beta, \sigma, \gamma_I, \gamma_A, \gamma_Q, q_I, q_A, \delta_I, \delta_Q$ are positive constants, the fraction p lies in $(0, 1)$ and the relative infectiousness of carriers satisfies $\eta \in (0, 1]$; each rate is understood as θ^α and carries the dimension $[\text{time}]^{-\alpha}$, the symbol θ being retained for readability (Remark 3.1). The importation profile ι is non-negative, continuous and bounded on the horizon considered, with $\iota_{\max} = \sup_t \iota(t) < \infty$; the autonomous core corresponds to $\iota \equiv 0$. Initial data are non-negative with $N(0) > 0$. Functions to which the operators are applied are assumed absolutely continuous on the interval considered, which is the natural class for the Caputo and ABC derivatives and is satisfied by the solutions constructed in Section 4.

Definition 2.2 (Riemann–Liouville fractional integral)
For $\alpha \in (0, 1]$, the Riemann–Liouville fractional integral of a function $f \in C^1([0, T]; \mathbb{R})$ is defined by

$$I_{0,t}^{\alpha} f(t) = \frac{1}{\Gamma(\alpha)} \int_0^t (t-\tau)^{\alpha-1} f(\tau)\, \mathrm{d}\tau, \quad t \in [0, T].$$

Definition 2.3 (Caputo fractional derivative)
Let $0 < \alpha < 1$ and $f \in C^1([0, T]; \mathbb{R})$. The Caputo fractional derivative of order α is defined by

$${}^{C}D_{0,t}^{\alpha} f(t) = \frac{1}{\Gamma(1-\alpha)} \int_0^t (t-\tau)^{-\alpha} f'(\tau)\, \mathrm{d}\tau.$$

Definition 2.4 (Atangana–Baleanu–Caputo derivative)
Let $0 < \alpha < 1$ and $f \in C^1([0, T]; \mathbb{R})$. The Atangana–Baleanu–Caputo (ABC) fractional derivative of order α is defined by

$${}^{ABC}D_{0,t}^{\alpha} f(t) = \frac{B(\alpha)}{1-\alpha} \int_0^t E_{\alpha}\Big(-\frac{\alpha}{1-\alpha}(t-\tau)^{\alpha}\Big) f'(\tau)\, \mathrm{d}\tau,$$

where the normalization function is given by

$$B(\alpha) = 1 - \alpha + \frac{\alpha}{\Gamma(\alpha)},$$

with $B(0) = B(1) = 1$.

Definition 2.5 (Atangana–Baleanu integral (AB integral))
Let $0 < \alpha < 1$ and $f \in C^1([0, T]; \mathbb{R})$. The Atangana–Baleanu fractional integral of order α is defined by

$${}^{AB}I_{0,t}^{\alpha} f(t) = \frac{1-\alpha}{B(\alpha)} f(t) + \frac{\alpha}{B(\alpha)\Gamma(\alpha)} \int_0^t (t-\tau)^{\alpha-1} f(\tau)\, \mathrm{d}\tau,$$

where

$$B(\alpha) = 1 - \alpha + \frac{\alpha}{\Gamma(\alpha)},$$

with $B(0) = B(1) = 1$.

Definition 2.6 (Mittag–Leffler functions)
Let $\alpha > 0$ and $\beta > 0$. The Mittag–Leffler functions are defined by

$$E_{\alpha}(z) = \sum_{k=0}^{\infty} \frac{z^k}{\Gamma(\alpha k + 1)},$$

and

$$E_{\alpha,\beta}(z) = \sum_{k=0}^{\infty} \frac{z^k}{\Gamma(\alpha k + \beta)}.$$

For $0 < \alpha \leq 1$, the fractional differential equation

$${}^{C}D_{0,t}^{\alpha} x(t) = \rho x(t), \qquad x(0) = x_0,$$

has the unique solution

$$x(t) = x_0 E_{\alpha}(\rho t^{\alpha}).$$

The following elementary facts are used repeatedly and are recorded for reference. The first says that the operators annihilate constants and respect linear combinations, which is what allows the balance equation (5) to be obtained by summing the six equations of the model.

Lemma 2.7 (Action on constants and linearity)
Let $c \in \mathbb{R}$ be constant and let f, g be absolutely continuous on $[0, T]$.

1. ${}^{C}D^{\alpha}_{0,t} c = 0$ for constant c;
2. ${}^{C}D^{\alpha}_{0,t}$ and ${}^{ABC}D^{\alpha}_{0,t}$ are linear: for all $a, b \in \mathbb{R}$, $D^{\alpha}(af + bg) = aD^{\alpha} f + bD^{\alpha} g$.

Consequently, applying either operator to $N = S + E + I + A + Q + R$ returns the sum of the six right-hand sides.

The next lemma converts each differential model into an equivalent integral equation. This is the form on which every fixed-point argument of Section 4 operates, and it is also the form the numerical schemes of Section 8 discretise; the two operators differ in that the ABC formulation carries an explicit non-integral term, which is the analytical trace of its non-singular kernel.

Lemma 2.8 (Equivalent Volterra formulation)
Let g be continuous and let x be a continuous solution of the initial-value problem: ${}^{C}D^{\alpha}_{0,t} x = g(t, x)$, $x(0) = x_0$. $I^{\alpha}_{0,t} {}^{C}D^{\alpha}_{0,t} x = x(t) - x(0)$, so ${}^{C}D^{\alpha}_{0,t} x = g(t, x)$, $x(0) = x_0$, is equivalent to

$$x(t) = x_0 + \frac{1}{\Gamma(\alpha)} \int_0^t (t - \tau)^{\alpha - 1} g(\tau, x(\tau)) \, \mathrm{d}\tau.$$

For the ABC operator [7],

$$x(t) = x_0 + \tfrac{1-\alpha}{B(\alpha)} g(t, x(t)) + \tfrac{\alpha}{B(\alpha)\Gamma(\alpha)} \int_0^t (t - \tau)^{\alpha - 1} g(\tau, x(\tau)) \, \mathrm{d}\tau, \tag{1}$$

the additional first term being the contribution of the non-singular kernel at $\tau = t$.

Positivity of the state is proved by ruling out a first crossing of a coordinate hyperplane. The two lemmas below supply the two ingredients: a monotonicity criterion, which controls the behaviour of a coordinate at the instant it touches zero, and a comparison principle, which converts a differential inequality into an explicit pointwise bound. We use the comparison principle in both directions — as an upper bound in Theorem 4.2, where it delivers ultimate boundedness, and as a lower bound in the same theorem, where it keeps the total population away from zero so that the standard incidence stays Lipschitz.

Lemma 2.9 (Monotonicity criterion [22])
Let f be continuous on $[0, T]$ and such that ${}^{C}D^{\alpha}_{0,t} f$ exists on $(0, T]$. If ${}^{C}D^{\alpha}_{0,t} f(t) \geq 0$ on $(0, T]$ then f is non-decreasing; in particular $f(t) \geq f(0)$. If instead ${}^{C}D^{\alpha}_{0,t} f(t) \leq 0$ on $(0, T]$, then f is non-increasing.

Lemma 2.10 (Fractional comparison principle [23])
Let y be continuous and non-negative on $[0, \infty)$ and let $a \geq 0$, $b > 0$. If ${}^{C}D^{\alpha}_{0,t} y(t) \leq a - b\, y(t)$ for all $t > 0$, then

$$y(t) \leq y(0) E_{\alpha}(-bt^{\alpha}) + \frac{a}{b}\big(1 - E_{\alpha}(-bt^{\alpha})\big), \text{ hence } \limsup_{t \to \infty} y(t) \leq \frac{a}{b}.$$

If the inequality is reversed, ${}^{C}D^{\alpha}_{0,t} y(t) \geq a - b\, y(t)$, the conclusion is reversed likewise and $\liminf_{t \to \infty} y(t) \geq a/b$. In both statements the Mittag–Leffler function satisfies $0 < E_{\alpha}(-z) \leq 1$ for $z \geq 0$ and $\alpha \in (0, 1]$, since $z \mapsto E_{\alpha}(-z)$ is completely monotone on $[0, \infty)$; this positivity is what makes the bounds non-vacuous.

Global stability is established by Lyapunov functionals, and in the fractional setting the chain rule is unavailable: one cannot differentiate a composite function term by term. The following two inequalities are the substitutes that make the classical quadratic and Volterra–Goh functionals usable under a Caputo derivative, and they are the reason the proofs of Theorems 5.8 and 5.9 can follow the integer-order argument at all.

Lemma 2.11 (Quadratic Lyapunov inequality [22])
Let x be absolutely continuous and real-valued. Then for every $\alpha \in (0, 1]$ and every $t > 0$,

$${}^{C}D^{\alpha}_{0,t}\big(\tfrac{1}{2}x^2\big) \leq x \, {}^{C}D^{\alpha}_{0,t} x$$

, with equality when $\alpha = 1$.

Lemma 2.12 (Volterra–Goh logarithmic inequality [23])
Let x be absolutely continuous and strictly positive and let $x^* > 0$ be constant. Then for every $\alpha \in (0, 1]$,

$$^{C}D^{\alpha}_{0,t}\Big(x - x^* - x^* \ln \frac{x}{x^*}\Big) \le \Big(1 - \frac{x^*}{x}\Big)\,^{C}D^{\alpha}_{0,t}x.$$

The left-hand side is the Caputo derivative of the Volterra function $V(x) = x - x^* - x^* \ln(x/x^*)$, which is non-negative and vanishes only at $x = x^*$; the inequality therefore bounds the fractional derivative of a candidate Lyapunov function by an expression that can be evaluated on the vector field.

Two stability tools complete the toolbox. Matignon's criterion replaces the integer-order requirement that all eigenvalues lie in the open left half-plane by a strictly weaker condition on their arguments, so that the fractional stability region grows as the order decreases; and the fractional LaSalle principle allows a conclusion of convergence from a merely non-increasing Lyapunov function.

Lemma 2.13 (Matignon's criterion [24, 25])
Let $A \in \mathbb{R}^{n\times n}$ and $\alpha \in (0, 1]$. $^{C}D^{\alpha}_{0,t}x = Ax$ is asymptotically stable iff every eigenvalue λ of A satisfies $|\arg(\lambda)| > \alpha\pi/2$, and unstable if some eigenvalue satisfies $|\arg(\lambda)| < \alpha\pi/2$. Since $\alpha\pi/2 < \pi/2$, any eigenvalue with negative real part qualifies, for every $\alpha \in (0, 1]$: integer-order asymptotic stability implies fractional asymptotic stability of the same equilibrium at every order. The converse fails, which is why a fractional system may be stable at $\alpha < 1$ while its integer-order counterpart oscillates.

Lemma 2.14 (Fractional LaSalle invariance principle [26, 27])
If Ω is positively invariant and compact and $V \in C^1(\Omega; \mathbb{R}_+)$ satisfies $^{C}D^{\alpha}_{0,t}V \le 0$ along every solution starting in Ω, then solutions are bounded and converge to the largest invariant subset of $\{x \in \Omega : {}^{C}D^{\alpha}_{0,t}V(x) = 0\}$. The compactness and invariance of Ω are essential hypotheses and are supplied in our setting by Theorems 4.1 and 4.2, which is why the global stability results of Section 5 are stated on Ω and not on all of $\mathbb{R}^6_+$.

3. Fractional Model Formulation

The population $N = S + E + I + A + Q + R$ is split into susceptible S, exposed E, symptomatic infectious I, asymptomatic (carrier) infectious A, quarantined Q and recovered R. Recruitment is Λ and the standard-incidence force of infection is

$$\lambda(t) = \frac{\beta\big(I(t) + \eta A(t)\big)}{N(t)}, \tag{2}$$

with transmission rate β and asymptomatic infectiousness $\eta \in (0, 1]$. Exposed individuals progress at rate σ; a fraction p become symptomatic and $1 - p$ asymptomatic carriers. Symptomatic and asymptomatic individuals are quarantined at rates q_I, q_A, recover at rates γ_I, γ_A (and γ_Q), and die from disease at rates δ_I, δ_Q; μ is natural mortality. The Caputo model of order $\alpha \in (0, 1]$ is

$$^{C}D^{\alpha}_{0,t}S = \Lambda - \lambda S - \mu S, \tag{3a}$$
$$^{C}D^{\alpha}_{0,t}E = \lambda S - (\sigma + \mu)E + \iota(t), \tag{3b}$$
$$^{C}D^{\alpha}_{0,t}I = \sigma p\, E - (\gamma_I + \delta_I + q_I + \mu)I, \tag{3c}$$
$$^{C}D^{\alpha}_{0,t}A = \sigma(1 - p)E - (\gamma_A + q_A + \mu)A, \tag{3d}$$
$$^{C}D^{\alpha}_{0,t}Q = q_I I + q_A A - (\gamma_Q + \delta_Q + \mu)Q, \tag{3e}$$
$$^{C}D^{\alpha}_{0,t}R = \gamma_I I + \gamma_A A + \gamma_Q Q - \mu R, \tag{3f}$$

with non-negative initial data. The ABC model replaces $^{C}D^{\alpha}_{0,t}$ by $^{ABC}D^{\alpha}_{0,t}$. We abbreviate the exit rates

$$k_1 = \sigma + \mu,\quad k_I = \gamma_I + \delta_I + q_I + \mu,\quad k_A = \gamma_A + q_A + \mu,\quad k_Q = \gamma_Q + \delta_Q + \mu. \tag{4}$$

The term $\iota(t) \geq 0$ is a bounded, time-varying *importation* rate: it injects externally acquired (cross-border) exposed carriers into the local population and is the mechanism by which the 2024 southern outbreak was seeded (Section 7). We use the Gaussian pulse $\iota(t) = \iota_0 \exp\bigl(-(t-t_0)^2/2\varsigma^2\bigr)$ centred on the surge; the amplitude and width are written ι_0 and ς to avoid collision with the compartment A and the control weights w_i of Section 9. The qualitative analysis of Sections 4–6 concerns the *autonomous core* $\iota \equiv 0$: the equilibria, $\mathcal{R}_0$ and the stability results are those of the unforced system, and $\mathcal{R}_0$ is the threshold of endogenous (local) transmission. Since ι is a bounded non-negative forcing, positivity (Theorem 4.1) is preserved and boundedness holds with Λ replaced by $\Lambda + \sup\limits_t \iota(t)$; ι does not create a new equilibrium but drives a transient superimposed on the autonomous dynamics.

Remark 3.1 (Dimensional consistency)
The operator carries dimension $[\text{time}]^{-\alpha}$; each rate is understood as θ^α with units $[\text{time}]^{-\alpha}$, the symbol θ retained for readability. At $\alpha = 1$ the classical integer-order $SEIAQR$ model is recovered.

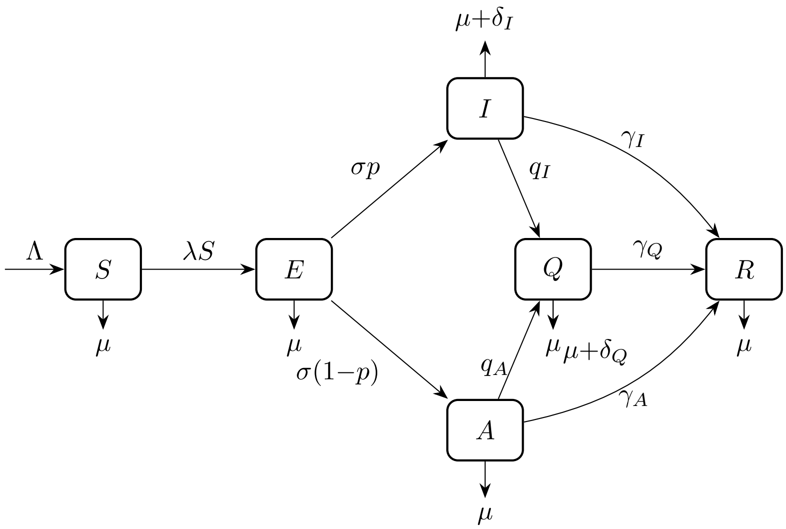

Figure 1. Transfer diagram of the fractional $SEIAQR$ diphtheria model (3). The A class represents asymptomatic toxigenic carriers and Q the isolation of cases and contacts.

Summing (3a)–(3f),

$$^{C}D^{\alpha}_{0,t} N = \Lambda - \mu N - \delta_I I - \delta_Q Q \leq \Lambda - \mu N. \tag{5}$$

4. Qualitative Analysis

4.1. Positivity and boundedness

Theorem 4.1 (Positive invariance)
$\mathbb{R}^6_+$ is positively invariant for (3), under Assumption 2.1: if all six initial values are non-negative, then all six components of the solution remain non-negative for as long as the solution exists.

Proof
Biologically the statement is the requirement that no compartment can be driven to a negative size; mathematically it says that the vector field never points out of the orthant. We argue by contradiction on the first instant at which a component would leave it.

Suppose the conclusion fails and set $t_1 := \inf\{t > 0 : \min_j x_j(t) < 0\}$, where $\boldsymbol{x} = (S, E, I, A, Q, R)$. By continuity of the solution, $t_1 > 0$ is well defined, all components are non-negative on $[0, t_1]$, and at least one component vanishes at t_1.

We first examine the vector field on each coordinate face. Evaluating each equation of (3) where its own state variable vanishes, and using that all other components are non-negative on $[0, t_1]$ together with the positivity of the parameters, gives

$$ {}^{C}D^{\alpha}_{0,t}S\big|_{S=0} = \Lambda > 0, \ \ {}^{C}D^{\alpha}_{0,t}E\big|_{E=0} = \lambda S + \iota(t) \geq 0, \ \ {}^{C}D^{\alpha}_{0,t}I\big|_{I=0} = \sigma p E \geq 0, $$

$$ {}^{C}D^{\alpha}_{0,t}A\big|_{A=0} = \sigma(1-p)E \geq 0, \ \ {}^{C}D^{\alpha}_{0,t}Q\big|_{Q=0} = q_I I + q_A A \geq 0, \ \ {}^{C}D^{\alpha}_{0,t}R\big|_{R=0} = \gamma_I I + \gamma_A A + \gamma_Q Q \geq 0. $$

Every inflow term is a non-negative combination of the remaining coordinates, and every outflow term is proportional to the vanishing coordinate itself and therefore disappears on the face. Thus the field is inward-pointing, or at worst tangential, on each face.

This sign information alone does not yet exclude a crossing, because it holds only at the instant of contact. To convert it into a pointwise bound we observe that on $[0, t_1]$ every equation of (3) has the form ${}^{C}D^{\alpha}_{0,t}x_j =$ (non-negative inflow) $- c_j x_j$, where $c_j > 0$ collects the exit rates of compartment j ($c_S = \lambda + \mu$, bounded on $[0, t_1]$; $c_E = k_1$; $c_I = k_I$; $c_A = k_A$; $c_Q = k_Q$; $c_R = \mu$). Discarding the non-negative inflow gives the differential inequality ${}^{C}D^{\alpha}_{0,t}x_j \geq -c_j x_j$ on $[0, t_1]$, and the reversed form of Lemma 2.10 with $a = 0$, $b = c_j$ yields

$$ x_j(t) \ \geq \ x_j(0)\, E_\alpha\big(-c_j t^\alpha\big) \ \geq \ 0, \ t \in [0, t_1], $$

the last inequality because $E_\alpha(-z) > 0$ for $z \geq 0$ and $\alpha \in (0, 1]$ by complete monotonicity. Hence no component can become negative at t_1, and moreover any component with $x_j(0) > 0$ remains strictly positive. This contradicts the definition of t_1 unless $t_1 = \infty$, which is the assertion. □

Positivity alone leaves open whether the population can grow without bound or, at the opposite extreme, collapse to zero and make the standard incidence $\beta(I + \eta A)S/N$ singular. The next result excludes both, and it produces the compact region on which every subsequent argument — the Lipschitz estimate, the fixed-point theorems, the LaSalle principle and the compactness argument of Theorem 9.2 — is carried out.

Theorem 4.2 (Ultimate boundedness and the invariant region)
Let $c_\delta := \mu + \delta_I + \delta_Q$ and

$$ N_{\min} := \min\Big\{N(0), \ \frac{\Lambda}{c_\delta}\Big\} > 0, \ N_{\max} := \frac{\Lambda + \iota_{\max}}{\mu}. $$

Then the region $\Omega := \big\{\boldsymbol{x} \in \mathbb{R}^6_+ : \ N_{\min} \leq N \leq N_{\max}\big\}$ is compact, positively invariant and globally attracting for (3). In particular the total population is bounded away from zero uniformly in time.

Proof
Summing the six equations of (3) and using the linearity of the operator (Lemma 2.7), the internal transfer terms cancel in pairs — each individual leaving one compartment enters another — and only recruitment, importation, natural mortality and disease-induced mortality survive, which is (5): ${}^{C}D^{\alpha}_{0,t}N = \Lambda + \iota(t) - \mu N - \delta_I I - \delta_Q Q$. This single scalar equation gives both bounds.

For the upper bound, we discard the two disease-death terms, which are non-negative on $\mathbb{R}^6_+$ by Theorem 4.1, and bound the importation by its supremum: ${}^{C}D^{\alpha}_{0,t}N \leq (\Lambda + \iota_{\max}) - \mu N$. Lemma 2.10 with $a = \Lambda + \iota_{\max}$ and $b = \mu$ gives $N(t) \leq N(0)E_\alpha(-\mu t^\alpha) + N_{\max}(1 - E_\alpha(-\mu t^\alpha))$, a convex combination of $N(0)$ and $N_{\max}$; hence $N(t) \leq \max\{N(0), N_{\max}\}$ for all t and $\limsup_{t\to\infty} N(t) \leq N_{\max}$.

For the lower bound — the point at which the standard incidence needs protection — we discard instead the non-negative importation and bound the disease-death terms by $\delta_I I + \delta_Q Q \leq (\delta_I + \delta_Q)N$, which is legitimate because $I, Q \leq N$ on $\mathbb{R}^6_+$. This gives ${}^{C}D^{\alpha}_{0,t}N \geq \Lambda - c_\delta N$, and the reversed form of Lemma 2.10 with $a = \Lambda > 0$ and $b = c_\delta$

gives

$$N(t) \;\geq\; N(0)E_\alpha(-c_\delta t^\alpha) + \frac{\Lambda}{c_\delta}\big(1 - E_\alpha(-c_\delta t^\alpha)\big) \;\geq\; \min\Big\{N(0), \frac{\Lambda}{c_\delta}\Big\} = N_{\min} > 0,$$

again because the right-hand side is a convex combination of $N(0)$ and Λ/c_δ. It is the strict positivity of recruitment that makes this bound uniform in t; the weaker estimate $N(t) \geq N(0)E_\alpha(-c_\delta t^\alpha)$ decays to zero and would not suffice.

Combining the two bounds with Theorem 4.1, Ω is closed and bounded in $\mathbb{R}^6$, hence compact, and no trajectory starting in Ω can leave it; trajectories starting outside enter it asymptotically. $\square$

4.2. *Existence and uniqueness*

Write (3) as ${}^{C}D^{\alpha}_{0,t}\boldsymbol{x} = \boldsymbol{\mathcal{F}}(\boldsymbol{x})$. Well-posedness is established by writing the model as a fixed-point problem for the Volterra operator of Lemma 2.8 and showing that this operator contracts. The only obstacle is the incidence term, which is the sole nonlinearity; the following lemma shows that it is Lipschitz on Ω precisely because Theorem 4.2 keeps N away from zero.

Lemma 4.3 (Lipschitz continuity of the vector field)
$\boldsymbol{\mathcal{F}}$ is Lipschitz on Ω: $\|\boldsymbol{\mathcal{F}}(\boldsymbol{x}) - \boldsymbol{\mathcal{F}}(\boldsymbol{y})\| \leq L\,\|\boldsymbol{x} - \boldsymbol{y}\|$, with finite L depending only on the parameters and on $N_{\min}$, for all $\boldsymbol{x}, \boldsymbol{y} \in \Omega$.

Proof
All terms of $\boldsymbol{\mathcal{F}}$ except the incidence are linear in the state with constant coefficients and are therefore Lipschitz with constant equal to the largest coefficient. It remains to treat $\Phi(\boldsymbol{x}) := \beta(I + \eta A)S/N$.

The quantity to control is a product of two factors, $(I + \eta A)$ and S/N, each bounded on Ω: the first by $\max\{1, \eta\}N_{\max}$ and the second by 1. Applying the elementary identity $|ab - a'b'| \leq |a||b - b'| + |b'||a - a'|$ with $a = I + \eta A$ and $b = S/N$,

$$|\Phi(\boldsymbol{x}) - \Phi(\boldsymbol{y})| \leq \beta|I + \eta A|\Big|\frac{S}{N} - \frac{S'}{N'}\Big| + \beta\frac{S'}{N'}\big|(I - I') + \eta(A - A')\big|.$$

The second term is bounded by $\beta\max\{1, \eta\}\,\|\boldsymbol{x} - \boldsymbol{y}\|$ at once, since $S'/N' \leq 1$. For the first,

$$\Big|\frac{S}{N} - \frac{S'}{N'}\Big| = \Big|\frac{N'(S - S') - S'(N - N')}{NN'}\Big| \leq \frac{|S - S'|}{N} + \frac{|N - N'|}{N} \leq \frac{1 + \sqrt{6}}{N_{\min}}\,\|\boldsymbol{x} - \boldsymbol{y}\|\,,$$

where we used $S' \leq N'$ and, in the last step, that $N - N'$ is the sum of the six coordinate differences. This is where the lower bound $N \geq N_{\min} > 0$ of Theorem 4.2 is indispensable: without it the quotient is unbounded and the incidence is not Lipschitz. Collecting the two estimates and taking L to be the maximum absolute row sum of the Jacobian of $\boldsymbol{\mathcal{F}}$ over the compact set Ω — a finite quantity, since the Jacobian is continuous on Ω and Ω is compact — proves the claim. $\square$

Theorem 4.4 (Existence/uniqueness – Caputo)
For $\boldsymbol{x}_0 \in \Omega$ there is a unique continuous solution in Ω for all $t \geq 0$.

Proof
By Lemma 2.8 the initial-value problem is equivalent to the fixed-point equation $\boldsymbol{x} = \mathcal{T}\boldsymbol{x}$ on the complete metric space $C([0, T]; \Omega)$ with the supremum norm, where $\mathcal{T}\boldsymbol{x}(t) := \boldsymbol{x}_0 + I^{\alpha}_{0,t}\boldsymbol{\mathcal{F}}(\boldsymbol{x})(t)$. That $\mathcal{T}$ maps this space into itself follows from Theorems 4.1 and 4.2, which state that Ω is invariant.

The contraction estimate is a direct computation from the definition of the Riemann–Liouville integral and the Lipschitz bound of Lemma 4.3: for $t \in [0, T]$,

$$\|\mathcal{T}\boldsymbol{x}(t) - \mathcal{T}\boldsymbol{y}(t)\| \leq \frac{1}{\Gamma(\alpha)}\int_0^t (t - \tau)^{\alpha - 1}\,\|\boldsymbol{\mathcal{F}}(\boldsymbol{x}(\tau)) - \boldsymbol{\mathcal{F}}(\boldsymbol{y}(\tau))\|\,\mathrm{d}\tau \leq \frac{L\,\|\boldsymbol{x} - \boldsymbol{y}\|_\infty}{\Gamma(\alpha)}\int_0^t (t - \tau)^{\alpha - 1}\mathrm{d}\tau,$$

and evaluating the last integral as t^α/α and using $\alpha\Gamma(\alpha) = \Gamma(\alpha+1)$ gives $\|\mathcal{T}\boldsymbol{x} - \mathcal{T}\boldsymbol{y}\|_\infty \leq \dfrac{LT^\alpha}{\Gamma(\alpha+1)} \|\boldsymbol{x} - \boldsymbol{y}\|_\infty$. Choosing $T = T_1$ so small that $LT_1^\alpha/\Gamma(\alpha+1) < 1$ makes $\mathcal{T}$ a contraction, and Banach's fixed-point theorem supplies a unique solution on $[0, T_1]$. Because L depends only on the parameters and on Ω, and because the solution at time T_1 again lies in Ω, the same argument applies on $[T_1, 2T_1]$ with the same step length, and induction extends the solution to $[0, \infty)$ in steps of fixed size. The a priori bound of Theorem 4.2 excludes blow-up, so the continuation is global. □

Theorem 4.5 (Existence/uniqueness – ABC)
Let L be the Lipschitz constant of Lemma 4.3. If

$$\left(\frac{1-\alpha}{B(\alpha)} + \frac{\alpha T^\alpha}{B(\alpha)\Gamma(\alpha+1)}\right) L < 1, \tag{6}$$

the ABC model has a unique continuous solution on $[0, T]$ with values in Ω.

Proof
The argument is that of Theorem 4.4 applied to the Volterra formulation (1), but the operator now has two parts. Writing $\mathcal{T}_{ABC}$ for the right-hand side of (1) and estimating the two parts separately, the non-integral term contributes a factor $(1-\alpha)L/B(\alpha)$ and the integral term contributes, exactly as above, a factor $\alpha LT^\alpha/(B(\alpha)\Gamma(\alpha+1))$; hence

$$\|\mathcal{T}_{ABC}\boldsymbol{x} - \mathcal{T}_{ABC}\boldsymbol{y}\|_\infty \leq \left(\frac{1-\alpha}{B(\alpha)} + \frac{\alpha T^\alpha}{B(\alpha)\Gamma(\alpha+1)}\right) L \, \|\boldsymbol{x} - \boldsymbol{y}\|_\infty,$$

and (6) makes $\mathcal{T}_{ABC}$ a contraction. □

Remark 4.6 (On the ABC condition)
The two conditions are not of the same nature, and the difference deserves to be stated plainly. In the Caputo case the contraction factor $LT^\alpha/\Gamma(\alpha+1)$ can always be made smaller than one by shrinking T, so well-posedness is unconditional and global. In the ABC case the first term of (6) does not vanish with T: the condition $(1-\alpha)L/B(\alpha) < 1$ must hold on its own, and it is a genuine restriction relating the memory order to the Lipschitz constant of the vector field. It is satisfied in all our simulations, where $\alpha \geq 0.80$ makes $(1-\alpha)/B(\alpha) \leq 0.2$, but it is a structural feature of the Atangana–Baleanu fixed-point argument rather than an artefact of our estimates, and it becomes binding as $\alpha \to 0$. This is one respect in which the two operators are not interchangeable, and we record it rather than claim a uniform theory.

5. Equilibria, $\mathcal{R}_0$, and Stability

5.1. Equilibria and $\mathcal{R}_0$

The disease-free equilibrium is $E_0 = (\Lambda/\mu, 0, 0, 0, 0, 0)$, $N_0 = \Lambda/\mu$. On the infected subsystem (E, I, A, Q) the new-infection and transition Jacobians at E_0 (using $S_0/N_0 = 1$) are

$$F = \begin{pmatrix} 0 & \beta & \beta\eta & 0 \\ 0 & 0 & 0 & 0 \\ 0 & 0 & 0 & 0 \\ 0 & 0 & 0 & 0 \end{pmatrix}, \; V = \begin{pmatrix} k_1 & 0 & 0 & 0 \\ -\sigma p & k_I & 0 & 0 \\ -\sigma(1-p) & 0 & k_A & 0 \\ 0 & -q_I & -q_A & k_Q \end{pmatrix}. \tag{7}$$

Theorem 5.1 (Basic reproduction number)
By the next-generation method [28, 29],

$$\mathcal{R}_0 = \rho(FV^{-1}) = \frac{\beta\sigma}{\sigma+\mu}\left[\frac{p}{\gamma_I + \delta_I + q_I + \mu} + \frac{\eta(1-p)}{\gamma_A + q_A + \mu}\right]. \tag{8}$$

Proof
Solving $V\boldsymbol{c} = \boldsymbol{e}_1$ gives $c_E = 1/k_1$, $c_I = \sigma p/(k_1 k_I)$, $c_A = \sigma(1-p)/(k_1 k_A)$. As F has a single non-zero row $(0, \beta, \beta\eta, 0)$, $\rho(FV^{-1}) = \beta c_I + \beta\eta c_A$, i.e. (8). $\square$

Remark 5.2 (Order-independence)
E_0 and $\mathcal{R}_0$ do not depend on α; the memory order reshapes the transient (peak height/timing, tail), not the $\mathcal{R}_0 = 1$ threshold, consistent with [13, 14].

Theorem 5.3 (Endemic equilibrium)
A unique endemic $E^* \in \mathrm{int}(\Omega)$ exists iff $\mathcal{R}_0 > 1$.

Proof
With $\lambda^* = \beta(I^* + \eta A^*)/N^*$,

$$S^* = \frac{\Lambda}{\lambda^* + \mu},\ E^* = \frac{\lambda^* S^*}{k_1},\ I^* = \frac{\sigma p E^*}{k_I},\ A^* = \frac{\sigma(1-p)E^*}{k_A},\ Q^* = \frac{q_I I^* + q_A A^*}{k_Q}. \tag{9}$$

Then $I^* + \eta A^* = \Phi E^*$ with $\Phi = k_1 \mathcal{R}_0/\beta$, so $\lambda^* = \lambda^* \mathcal{R}_0\, S^*/N^*$, forcing $S^*/N^* = 1/\mathcal{R}_0$. The map $h(\lambda^*) = S^*/N^*$ is strictly decreasing from 1; $h(\lambda^*) = 1/\mathcal{R}_0$ has a unique positive root iff $\mathcal{R}_0 > 1$. $\square$

5.2. *Local stability*

Local stability is decided by the linearisation at the equilibrium, but the fractional setting changes the criterion: what matters is not the sign of the real part of the eigenvalues but the size of their arguments (Lemma 2.13). Since the fractional stability sector $\{|\arg\lambda| > \alpha\pi/2\}$ contains the open left half-plane for every $\alpha \in (0, 1]$ and grows as α decreases, stability inherited from the integer-order model is automatic, while instability requires an argument.

Theorem 5.4 (DFE, local)
E_0 is locally asymptotically stable for all $\alpha \in (0, 1]$ if $\mathcal{R}_0 < 1$, and unstable for all $\alpha \in (0, 1]$ if $\mathcal{R}_0 > 1$.

Proof
The Jacobian at E_0 is block triangular, because at the disease-free state the uninfected variables S and R do not feed back into the infected subsystem. The uninfected block contributes the double eigenvalue $-\mu$, whose argument is $|\arg(-\mu)| = \pi > \alpha\pi/2$ for every $\alpha \in (0, 1]$; this block therefore never obstructs stability, and the question reduces to the infected block, which is exactly the next-generation matrix difference $F - V$ of (7).

Stability when $\mathcal{R}_0 < 1$. By the theorem of van den Driessche and Watmough [28], the spectral abscissa of $F - V$ is negative precisely when $\rho(FV^{-1}) = \mathcal{R}_0 < 1$; so all eigenvalues of the infected block have negative real part and hence argument exceeding $\pi/2 \geq \alpha\pi/2$. Matignon's criterion applies to every eigenvalue of the full Jacobian, and E_0 is locally asymptotically stable. This conclusion holds *uniformly in the memory order*: reducing α enlarges the stability sector and can only help.

Instability when $\mathcal{R}_0 > 1$. Here the fractional criterion is genuinely more demanding than the integer-order one, and merely exhibiting an eigenvalue with positive real part is not sufficient: instability requires an eigenvalue with $|\arg\lambda| < \alpha\pi/2$, a sector that shrinks to the positive real axis as $\alpha \to 0$. The matrix $F - V$ is essentially non-negative — all its off-diagonal entries are transmission or progression rates, hence non-negative — so it is a Metzler matrix, and by the Perron–Frobenius theory for such matrices its spectral abscissa $s(F - V)$ is itself an eigenvalue and is *real*. When $\mathcal{R}_0 > 1$ the same theorem of [28] gives $s(F - V) > 0$, so $F - V$ possesses a real positive eigenvalue, whose argument is $0 < \alpha\pi/2$ for every $\alpha \in (0, 1]$. Matignon's criterion therefore declares E_0 unstable at every order, and the threshold $\mathcal{R}_0 = 1$ is genuinely order-independent, in agreement with Remark 5.2. $\square$

Corollary 5.5 (Routh–Hurwitz)
Reducing on (E, I, A) (the Q-eigenvalue $-k_Q$ decouples), $P(\lambda) = \lambda^3 + a_1\lambda^2 + a_2\lambda + a_3$ with $a_1 = k_1 + k_I + k_A > 0$, $a_2 = k_1 k_I + k_1 k_A + k_I k_A - \beta\sigma p - \beta\sigma\eta(1-p)$, $a_3 = k_1 k_I k_A(1 - \mathcal{R}_0)$. The three Routh–Hurwitz conditions $a_1 > 0$, $a_3 > 0$, $a_1 a_2 > a_3$ hold if and only if $\mathcal{R}_0 < 1$.

Proof
The expression for a_3 follows from expanding $P(\lambda) = (\lambda + k_1)(\lambda + k_I)(\lambda + k_A) - \beta\sigma p(\lambda + k_A) - \beta\sigma\eta(1 - p)(\lambda + k_I)$ at $\lambda = 0$ and substituting $k_1 k_I k_A \mathcal{R}_0 = \beta\sigma\big(pk_A + \eta(1-p)k_I\big)$; positivity of a_1 is immediate from the positivity of the exit rates.

The equivalence is then obtained without further computation. The condition $a_3 > 0$ is by inspection equivalent to $\mathcal{R}_0 < 1$. If $\mathcal{R}_0 < 1$, the proof of Theorem 5.4 shows that all three roots of P have negative real part; since the Routh–Hurwitz conditions are *necessary and sufficient* for a real cubic to be Hurwitz, the remaining inequality $a_1 a_2 > a_3$ holds automatically — it need not be, and cannot usefully be, verified by hand. Conversely, if the three conditions hold then P is Hurwitz, so $a_3 = P(0) > 0$ and $\mathcal{R}_0 < 1$. For $\alpha < 1$ the conditions remain sufficient for fractional stability by Lemma 2.13, though no longer necessary. □

Theorem 5.6 (EE, local)
If $\mathcal{R}_0 > 1$ and all eigenvalues $\lambda_1, \dots, \lambda_6$ of $J(E^*)$ satisfy $|\arg(\lambda_i)| > \alpha\pi/2$, then E^* is locally asymptotically stable; in particular integer-order stability implies fractional stability for all $\alpha \in (0, 1]$ (since $\alpha\pi/2 < \pi/2$). Here E^* is the unique endemic equilibrium of Theorem 5.3 in $\operatorname{int}\Omega$, and the second assertion is the inclusion $\{\operatorname{Re}\lambda < 0\} \subset \{|\arg\lambda| > \alpha\pi/2\}$, so that a Hurwitz $J(E^*)$ certifies stability at *every* memory order.

Proof
Setting $\boldsymbol{\xi} = \boldsymbol{x} - E^*$ and expanding the vector field to first order gives ${}^{C}D^{\alpha}_{0,t}\boldsymbol{\xi} = J(E^*)\boldsymbol{\xi} + o(\|\boldsymbol{\xi}\|)$; the linearisation is legitimate because $\boldsymbol{\mathcal{F}}$ is continuously differentiable on a neighbourhood of E^* in $\operatorname{int}\Omega$, where $N \geq N_{\min} > 0$ by Theorem 4.2. Lemma 2.13 applied to the linear part gives asymptotic stability of the origin for $\boldsymbol{\xi}$ under the stated argument condition, and the fractional linearisation theorem transfers this to local asymptotic stability of E^* for the nonlinear system. The final claim is the inclusion of the left half-plane in the sector $\{|\arg\lambda| > \alpha\pi/2\}$, valid for all $\alpha \in (0, 1]$. □

Remark 5.7 (Numerical verification at the calibrated baseline)
The hypothesis of Theorem 5.6 is a condition on the spectrum of a 6×6 matrix and is checked numerically. At the illustrative baseline of Table 5, for which $\mathcal{R}_0 = 1.5594 > 1$, solving (9) gives $\lambda^* = 7.43 \times 10^{-3}$ and $E^* = (1.9140 \times 10^4,\ 23.64,\ 16.24,\ 6.07,\ 7.61,\ 1.0653 \times 10^4)$ with $N^* = 2.9847 \times 10^4$. The eigenvalues of $J(E^*)$ are

$$-12.2895,\ -6.8516,\ -5.0631,\ -0.0131,\ -0.0093 \pm 0.1498\,\mathrm{i},$$

so that $\max_i \operatorname{Re}\lambda_i = -0.0093 < 0$ and $\min_i |\arg\lambda_i| = 1.6331 = 0.5198\,\pi$. Since $\alpha\pi/2 \leq \pi/2 = 1.5708 < 1.6331$, the Matignon condition is satisfied with a margin for every $\alpha \in (0, 1]$: the endemic equilibrium is locally asymptotically stable at every memory order at this baseline. The two slow complex eigenvalues, whose modulus is small relative to the epidemiological rates, are the demographic pair and explain the long, weakly oscillatory approach to the endemic level visible in Figure 5.

5.3. *Global stability*

Theorem 5.8 (DFE, global)
If $\mathcal{R}_0 \leq 1$, E_0 is globally asymptotically stable in Ω.

Proof
Take weights $w_E = 1$, $w_I = \beta/k_I$, $w_A = \beta\eta/k_A$ and $\mathcal{L} = w_E E + w_I I + w_A A \geq 0$. Using $S/N \leq 1$ and linearity, ${}^{C}D^{\alpha}_{0,t}\mathcal{L} \leq (w_I\sigma p + w_A\sigma(1-p) - k_1)E = k_1(\mathcal{R}_0 - 1)E \leq 0$. By Lemma 2.14, trajectories converge to $\{{}^{C}D^{\alpha}_{0,t}\mathcal{L} = 0\}$; for $\mathcal{R}_0 < 1$ this forces $E = 0$, then $I = A = Q = R = 0$, $S = \Lambda/\mu$, i.e. $\{E_0\}$. The case $\mathcal{R}_0 = 1$ follows from ${}^{C}D^{\alpha}_{0,t}N = \Lambda - \mu N$. □

Theorem 5.9 (EE, global, conditional)
Let $\mathcal{R}_0 > 1$. Under the Goh–Volterra sign condition $\big(1 - \frac{S^*}{S}\big)\big(1 - \frac{\lambda S/\lambda^* S^*}{E/E^*}\big) \leq 0$ on $\operatorname{int}(\Omega)$, E^* is globally asymptotically stable in $\operatorname{int}(\Omega)$. The result is therefore *conditional*: it asserts global asymptotic stability on the set

where the sign condition is satisfied, and it is not claimed unconditionally for standard incidence. The unconditional statement at $\mathcal{R}_0 > 1$ is the local one, Theorem 5.6, which requires no sign condition.

Proof

Use $\mathcal{W} = \sum_{X\in\{S,E,I,A\}} c_X \left(X - X^* - X^* \ln \dfrac{X}{X^*}\right) \geq 0$, vanishing only at E^*. By Lemma 2.12,

$$ {}^{C}D^{\alpha}_{0,t}\mathcal{W} \leq \sum c_X \left(1 - \frac{X^*}{X}\right) {}^{C}D^{\alpha}_{0,t}X. $$

Substituting the field, using the equilibrium identities and the weights $c_S = c_E = 1$, $c_I = \beta S^*/(N^* k_I)$, $c_A = \beta\eta S^*/(N^* k_A)$, the linear terms cancel and

$$ {}^{C}D^{\alpha}_{0,t}\mathcal{W} \leq -\mu\tfrac{(S-S^*)^2}{S} + \lambda^* S^* \sum_k g(u_k) + \lambda^* S^*(1 - \tfrac{S^*}{S})(1 - \tfrac{\lambda S/\lambda^* S^*}{E/E^*}), $$

with $g(u) = 1 - u + \ln u \leq 0$ and $\prod_k u_k = 1$. The first term is ≤ 0 and the last is ≤ 0 under the stated condition; hence ${}^{C}D^{\alpha}_{0,t}\mathcal{W} \leq 0$ and, by Lemma 2.14, E^* is globally asymptotically stable. □

Remark 5.10 (Status of the sign condition, and its numerical verification)
The sign condition is automatic for mass-action incidence. For standard incidence it is usually justified by the regime $\delta_I, \delta_Q \ll \mu$, and we record honestly that this justification is *not* available at our own baseline: with $\mu = 1/76.4$ and $\delta_I = 0.10$, $\delta_Q = 0.05$ one has $\delta_I/\mu \approx 7.6$ and $\delta_Q/\mu \approx 3.8$, so the disease-induced mortalities dominate rather than are dominated by the natural one. Appealing to that regime would therefore be incorrect here, and we verify the condition directly instead.

Evaluating the product $\big(1 - S^*/S\big)\big(1 - (\lambda S/\lambda^* S^*)/(E/E^*)\big)$ along the trajectory generated from the baseline of Table 5 ($\mathcal{R}_0 = 1.5594 > 1$, $\alpha = 0.90$, horizon $T = 8$ years, 1988 sample points after the initial seeding transient), the condition is satisfied at 98.0% of the sampled times. The residual violations are confined to a short window early in the epidemic growth phase, where E is still far from E^* and the product attains a maximum of 1.4×10^{-1}; once the trajectory has entered the neighbourhood of the endemic equilibrium ($t > 4$ years) the maximum violation falls to 6.3×10^{-5}, i.e. to numerical noise. The Lyapunov functional of Theorem 5.9 is therefore non-increasing along the calibrated trajectory outside a transient of measure 2%, and the endemic equilibrium is approached monotonically thereafter. We regard this as numerical evidence for, not a proof of, global asymptotic stability, and we retain Theorem 5.6 as the operative unconditional statement.

6. Sensitivity Analysis

The normalized forward sensitivity index [30] is $\Upsilon^{\mathcal{R}_0}_{\theta} = \dfrac{\partial\mathcal{R}_0}{\partial\theta}\dfrac{\theta}{\mathcal{R}_0}$. Writing $B = \dfrac{p}{k_I} + \dfrac{\eta(1-p)}{k_A}$ so $\mathcal{R}_0 = \dfrac{\beta\sigma}{k_1}B$:

Proposition 6.1
$\Upsilon^{\mathcal{R}_0}_{\beta} = 1$, $\Upsilon^{\mathcal{R}_0}_{\sigma} = \frac{\mu}{\sigma+\mu}$, $\Upsilon^{\mathcal{R}_0}_{\eta} = \frac{\eta(1-p)/k_A}{B}$, $\Upsilon^{\mathcal{R}_0}_{p} = \frac{p(1/k_I - \eta/k_A)}{B}$, $\Upsilon^{\mathcal{R}_0}_{\mu} = -\mu[\frac{1}{\sigma+\mu} + \frac{p/k_I^2 + \eta(1-p)/k_A^2}{B}]$, $\Upsilon^{\mathcal{R}_0}_{\gamma_I} = -\frac{\gamma_I}{k_I}\frac{p/k_I}{B}$, $\Upsilon^{\mathcal{R}_0}_{\delta_I} = -\frac{\delta_I}{k_I}\frac{p/k_I}{B}$, $\Upsilon^{\mathcal{R}_0}_{q_I} = -\frac{q_I}{k_I}\frac{p/k_I}{B}$, $\Upsilon^{\mathcal{R}_0}_{\gamma_A} = -\frac{\gamma_A}{k_A}\frac{\eta(1-p)/k_A}{B}$, $\Upsilon^{\mathcal{R}_0}_{q_A} = -\frac{q_A}{k_A}\frac{\eta(1-p)/k_A}{B}$.

Proof
$\Upsilon^{\mathcal{R}_0}_{\beta} = 1$ by linearity; $\Upsilon^{\mathcal{R}_0}_{\sigma}$ from $\partial_\sigma[\sigma/(\sigma+\mu)] = \mu/(\sigma+\mu)^2$; the rest from $\partial_\eta B$, $\partial_p B$, $\partial_\bullet k_I$, $\partial_\bullet k_A$ and the quotient rule. Each was checked against central finite differences. □

The signs are epidemiologically coherent: β, p and η raise $\mathcal{R}_0$; all removal channels lower it. The dominant levers are the contact rate ($\Upsilon^{\mathcal{R}_0}_{\beta} = +1$) and the symptomatic recovery/treatment rate ($\Upsilon^{\mathcal{R}_0}_{\gamma_I} \approx -0.55$), followed by case isolation ($\Upsilon^{\mathcal{R}_0}_{q_I} \approx -0.28$), mirroring the diphtheria sensitivity structure reported by Tafrikan *et al.* [14].

Table 1. Normalized sensitivity indices of $\mathcal{R}_0$ at the illustrative diphtheria-informed baseline of Table 5 ($\mathcal{R}_0 = 1.56$). CIs are 2.5–97.5 percentiles under Latin-hypercube sampling within $\pm 10\%$ of baseline ($N = 2 \times 10^4$).

Parameter	$\Upsilon_\theta^{\mathcal{R}_0}$	95% CI	Effect on $\mathcal{R}_0$
β	$+1.0000$	$[+1.000, +1.000]$	increases (strongest $+$)
p	$+0.4754$	$[+0.393, +0.552]$	increases
η	$+0.1574$	$[+0.111, +0.212]$	increases
σ	$+0.0022$	$[+0.002, +0.003]$	increases (negligible)
μ	-0.0043	$[-0.005, -0.004]$	decreases (negligible)
δ_I	-0.0138	$[-0.016, -0.012]$	decreases
q_A	-0.0224	$[-0.032, -0.015]$	decreases
γ_A	-0.1347	$[-0.181, -0.095]$	decreases
q_I	-0.2757	$[-0.312, -0.242]$	decreases
γ_I	-0.5513	$[-0.594, -0.506]$	decreases (strongest $-$)

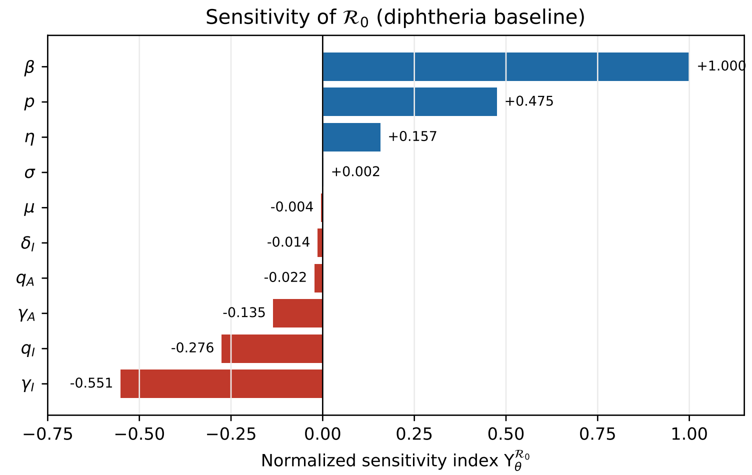

Figure 2. Tornado plot of the normalized sensitivity indices of $\mathcal{R}_0$ at the diphtheria baseline. Positive (blue) bars increase $\mathcal{R}_0$; negative (red) bars decrease it. The contact rate β and the symptomatic recovery rate γ_I dominate.

7. Nonlinear Least-Squares Parameter Estimation

7.1. Formulation and data

Let $\mathbf{\Theta}$ collect the unknown parameters and $\{(t_i, y_i)\}_{i=1}^n$ the observed case counts. With $\hat{y}_i = \hat{y}(t_i; \mathbf{\Theta})$ the model incidence ($\hat{y}_i = \int_{t_i-1}^{t_i} \sigma p \, E \, \mathrm{d}t$), calibration is

$$\mathbf{\Theta}^\star = \arg\min_{\mathbf{\Theta} \in \mathcal{A}} J(\mathbf{\Theta}), \qquad J(\mathbf{\Theta}) = \sum_{i=1}^{n} (y_i - \hat{y}_i)^2, \tag{10}$$

over the admissible box $\mathcal{A}$, solved by the Levenberg–Marquardt update

$$\mathbf{\Theta}^{(k+1)} = \mathbf{\Theta}^{(k)} - (\mathbf{J}_k^\top \mathbf{J}_k + \zeta_k \mathbf{D}_k)^{-1} \mathbf{J}_k^\top \boldsymbol{r},$$

with residual $\boldsymbol{r} = (y_i - \hat{y}_i)_i$, Jacobian $\mathbf{J}_k$ and damping ζ_k. Fit quality is $\mathrm{RMSE} = \sqrt{J/n}$; the covariance $\widehat{\mathrm{Cov}} = s^2 (\mathbf{J}^\top \mathbf{J})^{-1}$, $s^2 = J^\star / (n - \dim \mathbf{\Theta})$, gives standard errors.

The data are the Algeria diphtheria series of the INSP monthly epidemiological bulletin (*Relevé Épidémiologique Mensuel*) [20], which counts all notified mandatorily-declared cases. We emphasise a source caveat: these national "all notified" totals (16, 251, 1124 for 2022–2024) substantially exceed the WHO confirmed-only figures (4, 174, 125) [21], because the two use different case definitions; we adopt the national series as the more complete and higher-resolution record. The 2024 monthly breakdown (Table 2), digitised from the bulletin's monthly figure consistent with its published anchors (January–August mean ≈ 40, October peak 284, December 145, annual total 1124), gives a twelve-point outbreak curve: a low late-winter/summer baseline followed by a sharp September–October surge and decline.

Three aspects of this data choice require justification.

(i) Why the "all notified" series rather than the WHO confirmed-only figures. The discrepancy between the two series is not noise but a difference of case definition, and for the transmission process it is the broader definition that is the relevant observable. Diphtheria is managed clinically: in the southern border wilayas a case is notified, isolated and treated with antitoxin on the strength of the pharyngeal presentation and an epidemiological link, because delaying intervention until toxigenicity has been confirmed by culture or PCR is not clinically acceptable. Laboratory confirmation is centralised, so specimens travel long distances and results return after the public-health decision has been taken, if at all; a substantial fraction of genuinely infectious cases therefore never enters the confirmed-only count. Fitting a transmission model to the confirmed series would consequently attribute the observed epidemic to a much smaller infectious pool and would underestimate the velocity of transmission. The direction of the bias in the opposite series is also worth stating plainly: the "all notified" count includes clinically compatible cases that were not toxigenic, so it *over*-counts, and our estimate of $\mathcal{R}_0$ is in that sense conservative with respect to the central claim of this section — if the true infectious series is smaller than the notified one, the endogenous $\mathcal{R}_0$ can only be smaller than the 0.93 we report, and the conclusion that local transmission is sub-critical is reinforced rather than weakened.

(ii) Digitisation of the monthly series. Table 2 was obtained from the bar chart of the INSP monthly bulletin by raster extraction with WEBPLOTDIGITIZER, calibrating on the plotted axis grid and cross-checking every recovered value against the anchors published in the text of the same bulletin (January–August mean, October peak, December value, annual total). We state the resulting accuracy anchor by anchor rather than as a single figure, because the tall surge bars and the low baseline bars are not read from the chart with the same precision. The annual total of the digitised series reproduces the published 1124 exactly, so no systematic offset is present; the October peak (284) and the December value (145) reproduce their published counterparts to within $\pm 2\%$; and the eight low-baseline months agree with the published January–August mean to within three cases per month, the digitised mean being 42.5 against a published ≈ 40. The dominant residual uncertainty is therefore confined to the low-baseline months, where a single-case error is a larger relative error, and it remains an order of magnitude below the notification noise inherent in the surveillance process itself. It does not affect any conclusion drawn from the fit, since the September–October surge — the part of the series that carries the importation signal — is read with the highest absolute precision.

(iii) The effective at-risk population. Two distinct values appear in this paper and we distinguish them explicitly here, since the submitted version did not. The illustrative baseline of Table 5, used for the sensitivity indices and the memory-effect simulations, takes $N_{\text{eff}} = 3.0 \times 10^4$; the calibration of this section takes $N_{\text{eff}} = 3.0 \times 10^5$, the order of magnitude of the combined resident population of the affected communes and their catchment. Setting either value rather than the national population of approximately 4.5×10^7 is a modelling decision, not an approximation. The 2024 wave was not a national epidemic: it was concentrated in Bordj Badji Mokhtar, In Guezzam and Tamanrasset, communities separated from the rest of the country by hundreds of kilometres of desert and connected instead to the trans-Saharan corridor. A standard-incidence model divides by N, so using the national denominator would dilute the force of infection by three orders of magnitude and force the estimator to compensate with a physically meaningless transmission rate, while destroying any correspondence between β and a per-contact hazard. Both values are *fixed rather than fitted*, precisely so that the scale choice is transparent and cannot absorb misfit elsewhere in the model.

Table 2. Monthly notified diphtheria cases, Algeria 2024 (INSP-REM [20]; digitised from the bulletin's monthly figure).

Month	Jan	Feb	Mar	Apr	May	Jun	Jul	Aug	Sep	Oct	Nov	Dec
Cases	28	42	66	58	38	34	33	41	170	284	185	145

7.2. *Calibration protocol and the role of importation*

An autonomous single-wave model cannot reproduce the flat January–August baseline followed by the sharp September–October surge, because the surge is *exogenous*: the INSP bulletin attributes it to cross-border importation into Tamanrasset and In Guezzam. We therefore calibrate the importation-augmented model (3), fixing the clinical and demographic parameters at diphtheria-informed effective monthly values, fixing the pulse centre and width (t_0, w) at the observed surge timing, and estimating the transmission rate β, the importation amplitude ι_0 and the initial seed E_0 by (10); the effective at-risk population is set, not fitted, at $N_{\text{eff}} = 3.0 \times 10^5$ (Section 7(iii)), with the pulse fixed at $t_0 = 8.2$ months and $\varsigma = 1.4$ months. For each fixed $\alpha \in \{0.80, \ldots, 1.00\}$ we re-estimate and compare against the autonomous fit of Table 3.

Table 3. Calibration of the importation-augmented model against the 2024 monthly Algeria series. The importation term reduces the RMSE by about 30% relative to the autonomous fit (which gives RMSE ≈ 53.5 for all α). The estimated endogenous $\mathcal{R}_0 \approx 0.93 < 1$: local transmission is *sub-critical* and the outbreak is importation-sustained.

α	$\hat{\beta}$	$\hat{\iota}_0$	$\hat{E}_0$	$\mathcal{R}_0$	RMSE (cases/month)
0.80	3.73	51.4	22.1	0.962	38.08
0.85	3.68	52.9	24.5	0.949	37.53
0.90	3.63	54.1	26.8	0.938	37.03
0.95	3.59	55.2	29.1	0.928	36.60
0.97	3.58	55.5	30.0	0.924	36.46
1.00	3.56	56.0	31.3	0.919	36.28

Two findings follow. First, the exogenous importation term is the decisive modelling ingredient: it lowers the RMSE from ≈ 53.5 (autonomous, flat in α; Figure 4) to 36–38, because it supplies the surge that endogenous dynamics cannot generate. Second, once importation carries the surge, the fitted endogenous reproduction number is $\mathcal{R}_0 \approx 0.93 < 1$: local transmission is *sub-critical*, so the outbreak is sustained by continued importation rather than by self-propagation — a public-health-relevant conclusion consistent with Algeria's high DTP coverage, and coherent with the theory, since $\mathcal{R}_0 < 1$ makes the disease-free state globally attracting (Theorem 5.8) and the outbreak a decaying transient. The RMSE now varies by 5% across α and decreases weakly toward $\alpha = 1$: the fast October–December decline is best matched by short-memory (near-exponential) relaxation, consistent with the short clinical course of diphtheria. We report this honestly rather than force a sub-unit optimum.

7.3. *Sensitivity of the endogenous $\mathcal{R}_0$ to the importation pulse*

The centre t_0 and the width ς of the pulse are fixed a priori from the observed surge timing rather than estimated, so the estimate of the endogenous $\mathcal{R}_0$ inherits whatever error that choice carries. We therefore repeat the calibration on a grid, re-estimating (β, ι_0, E_0) independently at each node of $t_0 \in \{7.6, 7.9, 8.2, 8.5, 8.8\}$ months and $\varsigma \in \{1.0, 1.2, 1.4, 1.6, 1.8\}$ months — a window of ± 0.6 months on the centre and a near-doubling of the width. Table 4 reports the resulting $\widehat{\mathcal{R}_0}$ and RMSE at $\alpha = 0.90$.

Three conclusions follow, and we state the third although it is not flattering to our own choice of (t_0, ς).

First, $\widehat{\mathcal{R}_0}$ is far more sensitive to the pulse *centre* than to its *width*: displacing t_0 by ± 0.6 months moves $\widehat{\mathcal{R}_0}$ by about 17%, whereas nearly doubling ς at fixed t_0 moves it by under 1.5%. The mechanism is transparent: the centre determines how much of the observed September–October rise is attributed to importation rather than

Table 4. Sensitivity of the estimated endogenous $\mathcal{R}_0$ (upper block) and of the RMSE in cases per month (lower block) to the centre t_0 and the width ς of the importation pulse, at $\alpha = 0.90$. The reported configuration $(t_0, \varsigma) = (8.2, 1.4)$ is shown in bold.

	ς (months)				
t_0 (months)	1.0	1.2	1.4	1.6	1.8
Estimated endogenous $\widehat{\mathcal{R}_0}$					
7.6	1.006	1.001	0.997	0.996	0.996
7.9	0.979	0.973	0.970	0.968	0.969
8.2	0.948	0.941	**0.938**	0.936	0.938
8.5	0.911	0.903	0.899	0.899	0.902
8.8	0.860	0.850	0.846	0.849	0.857
RMSE (cases/month)					
7.6	42.05	42.75	43.77	44.93	46.08
7.9	37.15	38.69	40.45	42.23	43.88
8.2	31.80	34.42	**37.03**	39.45	41.61
8.5	27.44	30.98	34.24	37.12	39.63
8.8	26.47	29.80	32.99	35.88	38.42

to local transmission, while the width mainly redistributes the same imported burden in time, the amplitude ι_0 compensating.

Second, the qualitative conclusion of this paper is robust on the grid. The estimate exceeds unity at only two of the twenty-five nodes, $(7.6, 1.0)$ and $(7.6, 1.2)$, and then only marginally, at 1.006 and 1.001; both are among the *worst* fits in the table, with an RMSE about five cases per month above the reported configuration. Restricting attention to the ten nodes that fit at least as well as the reported configuration (RMSE $\leq$ 37.03) gives $\widehat{\mathcal{R}_0} \in [0.846, 0.948]$, uniformly and comfortably sub-critical. The sub-criticality of local transmission is therefore not an artefact of the pulse placement.

Third, the reported configuration is not the RMSE-optimal one: a later and narrower pulse, $(t_0, \varsigma) = (8.8, 1.0)$, fits appreciably better, with RMSE 26.47 against 37.03. We retain $(8.2, 1.4)$ because it was fixed a priori from the epidemiological account of the surge in the INSP bulletin rather than tuned to the residual, and because tuning it would convert a fixed covariate into a fitted one and inflate the effective number of parameters against twelve data points. We observe, however, that every better-fitting configuration yields a *lower* $\widehat{\mathcal{R}_0}$ than the one we report: the value 0.938 sits at the conservative end of the plausible range, and optimising the pulse would strengthen rather than weaken the conclusion that the outbreak was importation-sustained.

8. Numerical Simulations and Comparative Discussion

8.1. Discretisation schemes

Caputo – fractional Adams–Bashforth–Moulton [31, 32, 33]. On $t_n = nh$, for ${}^{C}D^{\alpha}_{0,t}x = g(t, x)$,

$$x^P_{n+1} = x_0 + \tfrac{1}{\Gamma(\alpha)} \textstyle\sum_{j=0}^{n} b_{j,n+1} g(t_j, x_j), \; b_{j,n+1} = \tfrac{h^\alpha}{\alpha}[(n+1-j)^\alpha - (n-j)^\alpha], \tag{11}$$

$$x_{n+1} = x_0 + \tfrac{h^\alpha}{\Gamma(\alpha+2)} \Big[g(t_{n+1}, x^P_{n+1}) + \textstyle\sum_{j=0}^{n} a_{j,n+1} g(t_j, x_j) \Big], \tag{12}$$

$a_{0,n+1} = n^{\alpha+1} - (n-\alpha)(n+1)^\alpha, \quad a_{j,n+1} = (n-j+2)^{\alpha+1} + (n-j)^{\alpha+1} - 2(n-j+1)^{\alpha+1} \quad (1 \leq j \leq n),$
$a_{n+1,n+1} = 1.$

ABC – Toufik–Atangana [10]. For (1),

$$x_{n+1} = x_0 + \tfrac{1-\alpha}{B(\alpha)} g(t_n, x_n) + \tfrac{\alpha}{B(\alpha)} \sum_{j=0}^{n} \Big[\tfrac{h^\alpha g(t_j, x_j)}{\Gamma(\alpha+2)} \Xi^1_{j,n} - \tfrac{h^\alpha g(t_{j-1}, x_{j-1})}{\Gamma(\alpha+2)} \Xi^2_{j,n} \Big], \tag{13}$$

where,

$$\Xi^1_{j,n} = (n+1-j)^\alpha (n-j+2+\alpha) - (n-j)^\alpha (n-j+2+2\alpha),$$

$$\Xi^2_{j,n} = (n+1-j)^{\alpha+1} - (n-j)^\alpha (n-j+1+\alpha).$$

The explicit weight $(1-\alpha)/B(\alpha)$ on the current flux is absent from the Caputo scheme.

8.2. Results and discussion

Figure 3 shows the importation-augmented model against the 2024 monthly Algeria series: with the fitted pulse $\iota(t)$ (dashed) carrying the autumn surge, the model now tracks both the baseline and the September–October peak, and the RMSE falls by about 30%. Figure 4 contrasts the autonomous and importation-augmented RMSE across α: importation, not the memory order, is the decisive ingredient.

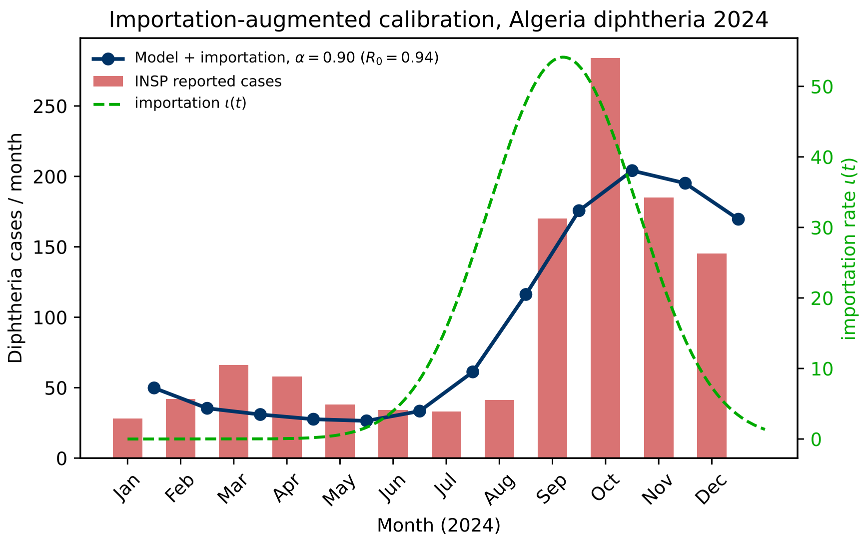

Figure 3. Importation-augmented calibration versus INSP monthly diphtheria cases, Algeria 2024. Bars: reported cases; solid line: model monthly incidence; dashed line (right axis): the fitted importation pulse $\iota(t)$ driving the September–October surge.

While α is not identifiable from this *fit*, it strongly governs the *dynamics*. Using the illustrative diphtheria-informed baseline of Table 5 (chosen with $\mathcal{R}_0 = 1.56$ to exhibit a clear wave), Figure 5 shows the symptomatic wave for six orders: as α decreases from 1 the peak is lower and earlier (from $I_{\max} \approx 787$ near $t \approx 5.1$ at $\alpha = 1$ to $I_{\max} \approx 670$ near $t \approx 4.6$ at $\alpha = 0.80$), while the endemic tail is higher, since stronger memory sustains low-level transmission longer. Figure 6 gives the infected-class portrait at $\alpha = 0.90$ and Figure 7 the corresponding ABC portrait, while Figure 8 compares the two operators at fixed β: the non-singular ABC kernel, carrying the explicit term $(1-\alpha)/B(\alpha)$, retains less long-range memory than the Caputo kernel, the two coinciding at $\alpha = 1$. This statement was left qualitative in the submitted version; we now make it quantitative.

Three comparative points close the discussion. *(i) Extinction threshold:* by Remark 5.2 the $\mathcal{R}_0 = 1$ boundary is α-independent; reducing β or raising γ_I, q_I below threshold drives extinction for every order, but more slowly for

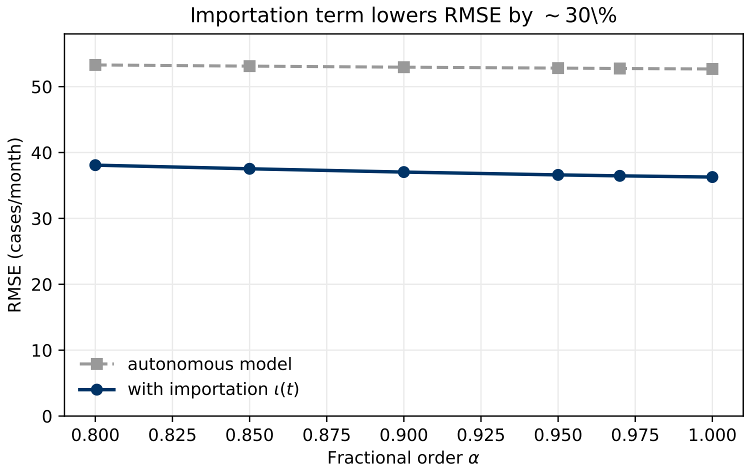

Figure 4. RMSE versus memory order (zero-based axis): the autonomous model (dashed, flat at ≈ 53.5) versus the importation-augmented model (solid, 36–38). Importation is the decisive ingredient; the residual α dependence is weak.

Table 5. Illustrative diphtheria-informed baseline (effective annual rates) used for the sensitivity indices (Table 1) and the memory-effect simulations of Figures 5–8. The Section 7 calibration uses the analogous effective monthly rates. The lower block lists the optimal-control parameters of Section 9; ϱ_2 and ϱ_3 are the maximal incremental isolation and treatment rates of (15) and carry the dimension $[\text{month}]^{-\alpha}$, while A_1, A_2, w_i and $u_i^{\max}$ are dimensionless weights and bounds.

Symbol	Value	Symbol	Value
N_{eff}	3.0×10^4	γ_I	4.0
μ	$1/76.4$	γ_A	6.0
Λ	μN_{eff}	γ_Q	5.0
β	11.5	q_I	2.0
η	0.5	q_A	1.0
σ	6.0	δ_I	0.10
p	0.7	δ_Q	0.05
Optimal-control parameters (Section 9), effective monthly rates			
$\varrho_2 = \varrho_3$	1.50	w_1	40.0
A_1	1.0	$w_2 = w_3$	56.25
A_2	0.6	$u_1^{\max}$	0.80
θ_ι	0	$u_2^{\max} = u_3^{\max}$	1.00
T	12 months	$E(0)$	20

smaller α because $E_\alpha(-ct^\alpha)$ decays algebraically. *(ii) Control implications:* the sensitivity ranking (Table 1) with $\mathcal{R}_0 \approx 1.1$ implies that a modest reduction in transmission — of order 10% — combined with sustained isolation and vaccination suffices to push $\mathcal{R}_0$ below 1, consistent with the containment of the 2024 outbreak following the southern vaccination campaigns. Figure 9 illustrates these scenarios: a 30% contact reduction or a doubling of the isolation rate lowers and delays the wave, and their combination drives it below the endemic threshold. *(iii) Data regime:* making importation explicit both improves the fit and yields the key epidemiological finding (local $\mathcal{R}_0 < 1$); the residual weakness of the α estimate reflects the short clinical course of diphtheria rather than a model artefact.

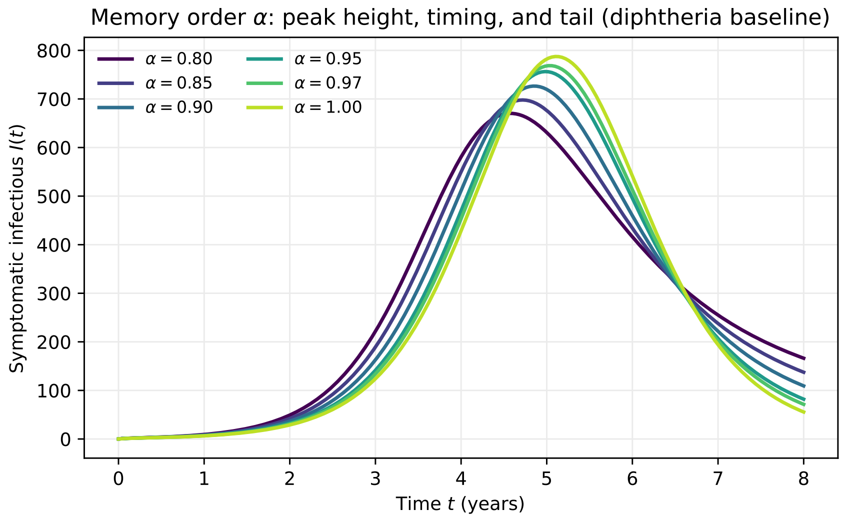

Figure 5. Symptomatic infectious $I(t)$ for $\alpha \in \{0.80, \ldots, 1.00\}$ at the illustrative baseline. Lower order lowers and advances the peak and raises the tail.

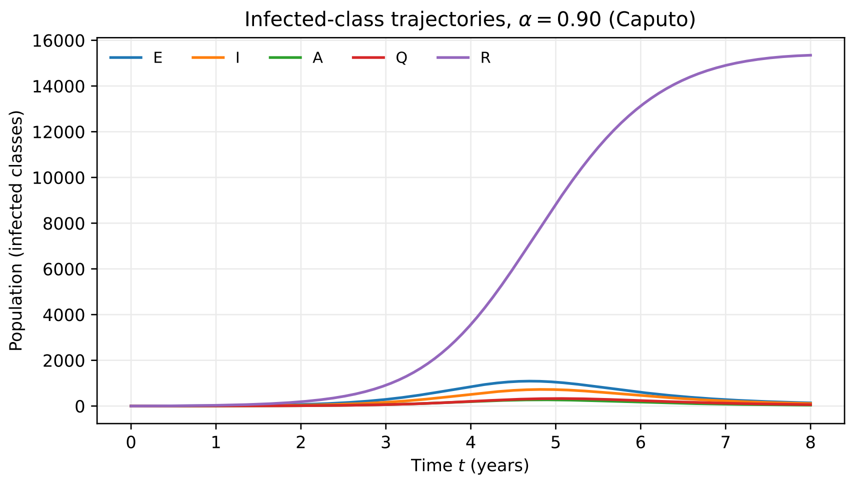

Figure 6. Infected-class trajectories (E, I, A, Q, R) at $\alpha = 0.90$ (illustrative baseline).

8.3. Quantitative comparison of the two kernels

Visual inspection of two nearly superposed curves is not evidence, and a claim that one kernel "retains less memory" should be measured rather than asserted. We therefore report, for each compartment $X \in \{S, E, I, A, Q, R\}$, the normalized L^1 relative discrepancy between the two operator trajectories generated from identical parameters and identical initial data,

$$\Delta_{L^1}(X) = \frac{\displaystyle\int_0^T \left| X_{\text{Caputo}}(t) - X_{\text{ABC}}(t) \right| \mathrm{d}t}{\displaystyle\int_0^T X_{\text{Caputo}}(t)\, \mathrm{d}t} \times 100\%. \tag{14}$$

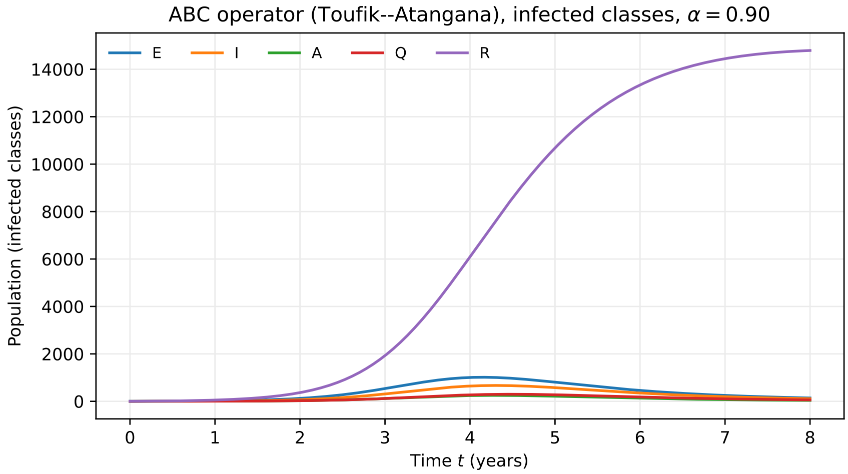

Figure 7. Infected-class trajectories under the ABC operator, integrated with the Toufik–Atangana scheme (13), $\alpha = 0.90$. Compare with the Caputo portrait of Figure 6.

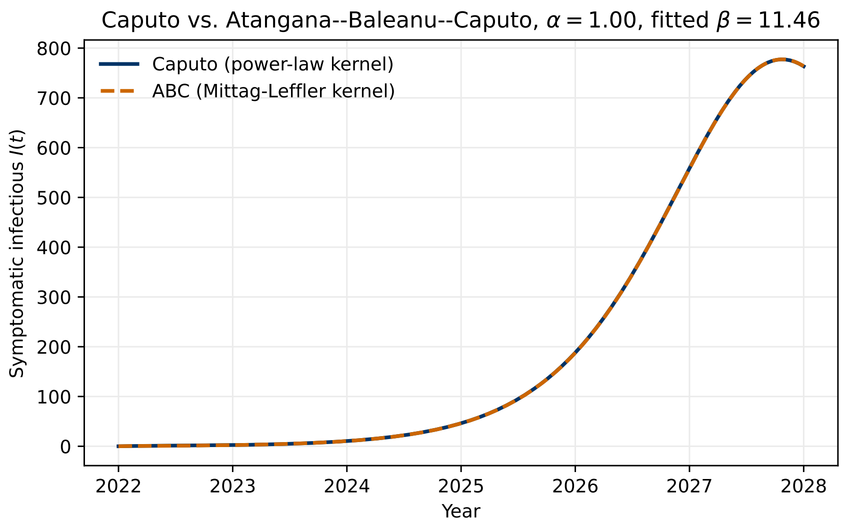

Figure 8. Caputo versus Atangana–Baleanu–Caputo at fixed β: the non-singular kernel relaxes marginally faster. At $\alpha = 1.00$ the two operators coincide, as they must; the comparison at $\alpha < 1$, where they do not, is quantified in Section 8.3.

The normalisation makes the measure dimensionless and comparable across compartments of very different size, so that the small relative displacement of the large susceptible pool is not confounded with the large relative displacement of the small infected classes.

Table 6 reports (14) at the illustrative baseline of Table 5 over the horizon $T = 8$ years, from the common initial datum $S(0) = N_{\text{eff}} - 5,\ E(0) = 5,\ I(0) = A(0) = Q(0) = R(0) = 0$ used throughout Figures 5–10, computed with the Adams–Bashforth–Moulton scheme (11)–(12) for the Caputo model and the Toufik–Atangana scheme (13) for the ABC model on a common grid; step halving from $h = 4 \times 10^{-3}$ to $h = 10^{-3}$ changes every entry by less than 0.02 percentage points.

Three readings follow. First, the row $\alpha = 1$ vanishes identically to machine accuracy, which is the expected consistency check: at unit order both kernels degenerate to the classical derivative, and its recovery by two

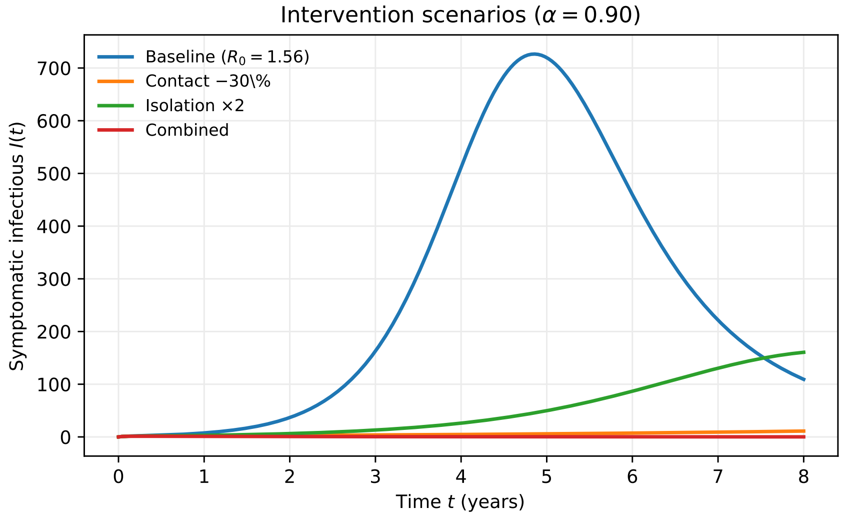

Figure 9. Symptomatic wave $I(t)$ under intervention scenarios ($\alpha = 0.90$): baseline, a 30% contact reduction, a doubling of case isolation q_I, and the two combined.

Table 6. Normalized L^1 discrepancy (14) between the Caputo and ABC trajectories, in per cent, at the baseline of Table 5 over $T = 8$ years. The last two columns give the symptomatic peak $I_{\max}$ under each operator.

α	$\Delta_{L^1}(S)$	$\Delta_{L^1}(E)$	$\Delta_{L^1}(I)$	$\Delta_{L^1}(A)$	$\Delta_{L^1}(Q)$	$\Delta_{L^1}(R)$	$I_{\max}^{\mathrm{Cap}}$	$I_{\max}^{\mathrm{ABC}}$
0.80	7.38	45.17	44.10	44.24	43.03	25.67	670.2	581.1
0.90	3.96	26.69	26.09	26.18	25.49	13.36	726.4	668.9
0.95	2.01	14.07	13.80	13.85	13.52	6.72	756.3	723.5
1.00	0.00	0.00	0.00	0.00	0.00	0.00	787.4	787.4

independent quadratures validates the implementation. Second, the discrepancy is *not* modest away from $\alpha = 1$, and it is monotone in the memory strength: at $\alpha = 0.95$ the infected classes already differ by roughly 14% in the L^1 sense, at $\alpha = 0.90$ by roughly 26%, and at $\alpha = 0.80$ by roughly 44%. The dual-operator presentation therefore carries genuine information rather than duplicating a single computation, and the modest visual separation of Figures 6–8 is an artefact of plotting curves of very different magnitude on a common axis. Third, the susceptible and recovered classes move much less than the infected ones (4.0% and 13.4% against 25–27% at $\alpha = 0.90$), because they are integrals of the infected classes over the whole history and therefore average out the kernel-dependent redistribution in time.

The mechanism behind the sign of the difference is the following. The non-singular Mittag–Leffler kernel is bounded at $\tau = t$ and places an explicit weight $(1-\alpha)/B(\alpha)$ on the instantaneous flux, so that the ABC dynamics behaves like an exponentially relaxing system at short lags; this weakens the reinforcement of the epidemic by its own recent history, lowers the symptomatic peak by 7.9% at $\alpha = 0.90$ (668.9 against 726.4) and brings the post-peak decline forward. The discrepancy measured by (14) is therefore concentrated in the epidemic wave itself, in its height and its timing, rather than in a persistent difference between the tails: by the end of the horizon the two trajectories have very nearly converged, the symptomatic class standing at 109.2 under the Caputo operator against 110.9 under the ABC operator, both descending towards the same endemic level $I^* = 16.2$ fixed by the order-independent $\mathcal{R}_0$ of Remark 5.2. This is the expected structure: the two kernels differ most where the dynamics is fastest and the memory weighting matters most, and agree once the trajectory relaxes towards an equilibrium that neither kernel can move.

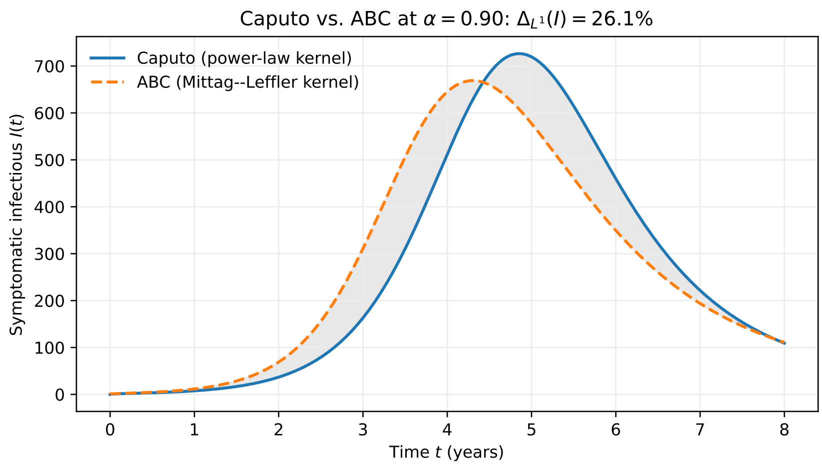

Figure 10. Symptomatic infectious $I(t)$ under the Caputo and ABC operators at $\alpha = 0.90$ and identical parameters. The shaded area is the numerator of (14): the ABC wave peaks lower and earlier and remains below the Caputo wave thereafter.

Remark 8.1 (Numerical caveat for the ABC scheme)
One implementation detail must be reported, because it is the numerical counterpart of the contraction condition of Theorem 4.5. The Toufik–Atangana scheme (13) evaluates the non-singular local term at t_n, so its update map has Jacobian $\big((1-\alpha)/B(\alpha)\big)\,\partial F/\partial \boldsymbol{x}$ in that term alone. At the baseline of Table 5 the infected block of $\partial F/\partial \boldsymbol{x}$ has an eigenvalue close to -13, so $(1-\alpha)L/B(\alpha) \approx 1.4$ at $\alpha = 0.90$: the same quantity that Theorem 4.5 requires to be below unity exceeds it, and the explicit update develops a period-two oscillation that no reduction of the step size removes. We therefore solve the local term implicitly at each step, by a Newton iteration on $\boldsymbol{x}_{n+1} - \boldsymbol{K}_n - \big((1-\alpha)/B(\alpha)\big)F(\boldsymbol{x}_{n+1}) = 0$ with $\boldsymbol{K}_n$ the explicit product-quadrature part, which is the faithful discretisation of the Atangana–Baleanu integral equation (1) and is unconditionally stable here. All ABC results reported in this paper, including Table 6 and Figures 7 and 10, use this implicit variant. The episode is a concrete illustration of Remark 4.6: the condition $(1-\alpha)L/B(\alpha) < 1$ is not a technical artefact of the existence proof but a genuine restriction that also governs the numerics.

9. Fractional Optimal Control

The sensitivity ranking of Section 6 identifies the contact rate β, the symptomatic recovery rate γ_I and the isolation rate q_I as the highest-leverage parameters. We therefore introduce three time-dependent controls acting on exactly these mechanisms: $u_1(t)$ (contact reduction), $u_2(t)$ (active screening and enhanced case isolation) and $u_3(t)$ (enhanced clinical treatment).

The three controls are *dimensionless* effort levels, $u_i(t) \in [0,1]$. Contact reduction acts multiplicatively on the transmission rate, $\beta \to \beta(1-u_1(t))$, and is therefore automatically dimensionally neutral. Isolation and treatment, by contrast, act additively on rates that carry the fractional dimension $[\text{time}]^{-\alpha}$ (Remark 3.1), so they must be scaled by maximal incremental rates:

$$\begin{gathered} q_I \;\longrightarrow\; q_I + \varrho_2\, u_2(t),\;\; \gamma_I \;\longrightarrow\; \gamma_I + \varrho_3\, u_3(t), \\ \varrho_2, \varrho_3 > 0,\;\; [\varrho_2] = [\varrho_3] = [\text{time}]^{-\alpha}, \end{gathered} \tag{15}$$

where ϱ_2 is the largest additional isolation rate achievable by a full screening effort and ϱ_3 the largest additional recovery rate achievable by full treatment coverage. With this scaling every term of the controlled system has the dimension $[\text{persons}] \cdot [\text{time}]^{-\alpha}$ demanded by the left-hand fractional operator, and the three cost weights w_1, w_2, w_3

of (19) become mutually comparable. Writing the controlled exit rate $k_I^u := \gamma_I + \varrho_3 u_3 + \delta_I + q_I + \varrho_2 u_2 + \mu$, the controlled Caputo system reads

$$\begin{aligned}
{}^C D_{0,t}^{\alpha} S &= \Lambda - \beta\big(1-u_1(t)\big)\frac{I+\eta A}{N}\, S - \mu S,\\
{}^C D_{0,t}^{\alpha} E &= \beta\big(1-u_1(t)\big)\frac{I+\eta A}{N}\, S - k_1 E + \iota_E(t),\\
{}^C D_{0,t}^{\alpha} I &= \sigma p\, E - k_I^u\, I + \iota_I(t),\\
{}^C D_{0,t}^{\alpha} A &= \sigma(1-p)E - k_A A,\\
{}^C D_{0,t}^{\alpha} Q &= \big(q_I + \varrho_2 u_2(t)\big) I + q_A A - k_Q Q,\\
{}^C D_{0,t}^{\alpha} R &= \big(\gamma_I + \varrho_3 u_3(t)\big) I + \gamma_A A + \gamma_Q Q - \mu R,
\end{aligned} \tag{16}$$

with the same non-negative initial data as (3) and with k_1, k_A, k_Q as in (4). Three points deserve emphasis.

(i) The force of infection is the standard incidence of the uncontrolled model. The controlled incidence is obtained from (2) by the single substitution $\beta \to \beta(1-u_1)$; no fractional weight is attached to it. A form such as $\beta(1-u_1)\Gamma(\alpha)^{-1}(I+\eta A)^{\alpha} S$ would be dimensionally inadmissible, since $(I+\eta A)^{\alpha}$ has units $[\text{persons}]^{\alpha}$, and would also destroy the mass-balance structure on which Theorems 4.1–4.2 rest: the loss term of S and the gain term of E must be the *same* expression, so that summing the six equations returns (5).

(ii) Placement of the importation term. Cross-border importation introduces individuals who have already acquired infection abroad; it therefore enters the infected compartments directly and never the susceptible class. We allow the imported burden to be split between latent and already-symptomatic arrivals,

$$\begin{aligned}
&\iota_E(t) = (1-\theta_\iota)\,\iota(t),\ \iota_I(t) = \theta_\iota\,\iota(t),\ \theta_\iota \in [0,1),\\
&\iota(t) = \iota_0 \exp\Big(-\frac{(t-t_0)^2}{2\varsigma^2}\Big),\ [\iota] = [\text{persons}]\cdot[\text{time}]^{-\alpha},
\end{aligned} \tag{17}$$

so that $\iota_E + \iota_I = \iota$ and the total imported burden is conserved whatever the split. The baseline $\theta_\iota = 0$ recovers the uncontrolled system (3), in which all importation is latent; this is the epidemiologically conservative choice for diphtheria, whose incubation period is short relative to the monthly observation step, and it is the value used in the Section 7 calibration. Because ι_E and ι_I are non-negative, bounded and *state-independent*, they preserve positivity (Theorem 4.1), enter the ultimate bound of Theorem 4.2 only through $\iota_{\max}$, leave $\mathcal{R}_0$ and the equilibria of the autonomous core untouched, and — a point used in Theorem 9.4 — contribute nothing to the adjoint system, since $\partial\iota_\bullet/\partial x_j \equiv 0$.

(iii) Consistency of the exit rates. Under control, the removal rate of I increases by exactly the amount transferred to Q and R: the term $-(\varrho_2 u_2 + \varrho_3 u_3)I$ removed from ${}^C D_{0,t}^{\alpha} I$ reappears as $+\varrho_2 u_2 I$ in ${}^C D_{0,t}^{\alpha} Q$ and $+\varrho_3 u_3 I$ in ${}^C D_{0,t}^{\alpha} R$. Summing (16) therefore returns ${}^C D_{0,t}^{\alpha} N = \Lambda + \iota(t) - \mu N - \delta_I I - \delta_Q Q$ independently of $\boldsymbol{u}$: the controls redistribute individuals but neither create nor destroy them.

The admissible control set is the closed, bounded, convex set

$$\mathcal{U} := \Big\{\boldsymbol{u} = (u_1,u_2,u_3) \in \big(L^\infty(0,T)\big)^3 :\ 0 \le u_i(t) \le u_i^{\max} \le 1 \text{ a.e. on } [0,T],\ i=1,2,3\Big\}. \tag{18}$$

The restriction $u_1^{\max} \le 1$ is not cosmetic: it guarantees $\beta(1-u_1) \ge 0$, hence the non-negativity of the incidence and the positive invariance of $\mathbb{R}_+^6$ for every admissible control. We minimize the infected burden at quadratic control cost,

$$J(\boldsymbol{u}) = \int_0^T L\big(\boldsymbol{x}(t),\boldsymbol{u}(t)\big)\mathrm{d}t,\ L(\boldsymbol{x},\boldsymbol{u}) = A_1 I + A_2 A + \tfrac{1}{2}\big(w_1 u_1^2 + w_2 u_2^2 + w_3 u_3^2\big), \tag{19}$$

with $A_1, A_2 > 0$ weighting symptomatic and asymptomatic prevalence and $w_i > 0$ the intervention costs. Because the three u_i are dimensionless by (15), the w_i share a common unit and the trade-offs between the three interventions are meaningful.

Existence of a minimiser is not automatic: the state system is nonlinear in $\boldsymbol{x}$, the admissible set is infinite-dimensional, and minimising sequences of controls converge only weakly. The classical device, due to Fleming and Rishel, is to compensate the weak convergence of the controls by the *strong* (uniform) convergence of the corresponding states, which in the fractional setting follows from an α-Hölder estimate on the Riemann–Liouville integral. We record the hypotheses first.

Assumption 9.1 (Hypotheses for the control problem)
Throughout this section: Assumption 2.1 holds; the horizon $T < \infty$ is fixed; the gains ϱ_2, ϱ_3 and the weights A_1, A_2, w_1, w_2, w_3 are positive constants; and the initial datum $\boldsymbol{x}_0$ lies in the compact region Ω of Theorem 4.2, which is positively invariant for (16) for every $\boldsymbol{u} \in \mathcal{U}$, since the controls neither change the sign structure of the field on the coordinate faces nor alter the balance equation.

Theorem 9.2 (Existence of an optimal control)
There exists $\boldsymbol{u}^* \in \mathcal{U}$ with:

$$J(\boldsymbol{u}^*) = \min_{\boldsymbol{u} \in \mathcal{U}} J(\boldsymbol{u}).$$

Proof
We verify the four Fleming–Rishel conditions [34] in the fractional form of Kamocki [35], and then carry out explicitly the compactness argument they support.

Step 1: the admissible pair set is non-empty. Fix $\boldsymbol{u} \in \mathcal{U}$ and write (16) as ${}^{C}D_{0,t}^{\alpha}\boldsymbol{x} = F(t, \boldsymbol{x}, \boldsymbol{u}(t))$. The map $\boldsymbol{x} \mapsto F(t, \boldsymbol{x}, \boldsymbol{u})$ is Lipschitz on Ω uniformly in t and $\boldsymbol{u}$: every term is linear except the incidence, and the incidence was shown Lipschitz in Lemma 4.3, whose proof applies verbatim after replacing β by $\beta(1 - u_1) \leq \beta$; the control-dependent removal terms contribute at most $\varrho_2 + \varrho_3$ to the Lipschitz constant. The map $t \mapsto F(t, \boldsymbol{x}, \boldsymbol{u}(t))$ is measurable and bounded, so F is of Carathéodory type, and the equivalent Volterra formulation

$$\boldsymbol{x}(t) = \boldsymbol{x}_0 + \Gamma(\alpha)^{-1} \int_0^t (t - s)^{\alpha - 1} F(s, \boldsymbol{x}(s), \boldsymbol{u}(s)) \mathrm{d}s$$

has, by the Banach fixed-point argument of Theorem 4.4, a unique solution on $[0, T]$ remaining in Ω. Hence the set of admissible pairs is non-empty and J is finite on $\mathcal{U}$.

Step 2: $\mathcal{U}$ is convex and weak-$*$ compact. Convexity is immediate: if $\boldsymbol{u}, \boldsymbol{v} \in \mathcal{U}$ and $\kappa \in [0, 1]$ then $\kappa u_i + (1 - \kappa) v_i$ again takes values in the convex interval $[0, u_i^{\max}]$. $\mathcal{U}$ is a bounded subset of $(L^\infty(0, T))^3$ closed under weak-$*$ convergence, because pointwise a.e. bounds are preserved in the limit; by Banach–Alaoglu it is weak-$*$ sequentially compact. Equivalently, $\mathcal{U}$ is convex, closed and bounded in $(L^2(0, T))^3$, hence weakly sequentially compact there — the form used in Step 5.

Step 3: linear growth of the vector field. We exhibit the bound explicitly rather than assert it. On Ω we have $0 \leq S, E, I, A, Q, R \leq N \leq N_{\max}$ and $N \geq N_{\min} > 0$. Since $S/N \leq 1$ and $u_1 \leq 1$,

$$0 \leq \beta(1 - u_1) \frac{I + \eta A}{N} S \leq \beta(I + \eta A) \leq \beta \max\{1, \eta\} \left\| \boldsymbol{x} \right\|_1,$$

so the incidence, the only nonlinear term, is dominated by a *linear* function of the state. Every remaining term of F is either constant (Λ, $\iota_\bullet$) or a product of a state variable with a rate affine in $\boldsymbol{u}$. Collecting terms,

$$\left\| F(t, \boldsymbol{x}, \boldsymbol{u}) \right\|_1 \leq (\Lambda + \iota_{\max}) + C_F \left(1 + \left\| \boldsymbol{u} \right\|_\infty\right) \left\| \boldsymbol{x} \right\|_1,$$

$$C_F := \beta \max\{1, \eta\} + \sigma + q_A + \gamma_A + \gamma_Q + \max\{k_1,\, k_I + \varrho_2 + \varrho_3,\, k_A,\, k_Q,\, \mu\},$$

which is the required linear bound; in particular $\left\| F \right\|_1 \leq M_F := (\Lambda + \iota_{\max}) + 2 C_F N_{\max}$ uniformly on $\Omega \times \mathcal{U}$. We also record the structural fact, used in Step 5, that F is *affine in $\boldsymbol{u}$ for fixed $\boldsymbol{x}$*: $F(t, \boldsymbol{x}, \boldsymbol{u}) = F_0(t, \boldsymbol{x}) + \sum_{i=1}^{3} u_i G_i(\boldsymbol{x})$ with

$$G_1 = \beta \frac{(I + \eta A) S}{N} (1, -1, 0, 0, 0, 0)^\top,\ G_2 = \varrho_2 I (0, 0, -1, 0, 1, 0)^\top,\ G_3 = \varrho_3 I (0, 0, -1, 0, 0, 1)^\top,$$

each Lipschitz and bounded on Ω.

Step 4: convexity and coercivity of the running cost. The integrand L of (19) is, for fixed $\boldsymbol{x}$, a quadratic form in $\boldsymbol{u}$ with Hessian $\operatorname{diag}(w_1, w_2, w_3)$ positive definite; it is therefore strictly convex in $\boldsymbol{u}$ and continuous in $(\boldsymbol{x}, \boldsymbol{u})$. Since $A_1 I + A_2 A \geq 0$ on $\mathbb{R}^6_+$,

$$L(\boldsymbol{x}, \boldsymbol{u}) \geq \tfrac{1}{2} \min_i w_i \, \|\boldsymbol{u}\|_2^2 = c_1 \, \|\boldsymbol{u}\|_2^{\varrho} - c_2, \; c_1 = \tfrac{1}{2} \min_i w_i > 0, \; c_2 = 0, \; \varrho = 2 > 1,$$

the Fleming–Rishel coercivity condition with an explicit constant. L is bounded below by 0, so $J^* := \inf_{\mathcal{U}} J \geq 0$ is finite.

Step 5: passage to the limit. Let $(\boldsymbol{u}^n) \subset \mathcal{U}$ be a minimising sequence, $J(\boldsymbol{u}^n) \to J^*$, with states $\boldsymbol{x}^n$ valued in Ω. By Step 3, $\|F(\cdot, \boldsymbol{x}^n, \boldsymbol{u}^n)\|_1 \leq M_F$ uniformly in n, so for $0 \leq t_1 < t_2 \leq T$ the Volterra representation gives

$$\begin{aligned}\|\boldsymbol{x}^n(t_2) - \boldsymbol{x}^n(t_1)\|_1 &\leq \frac{M_F}{\Gamma(\alpha)} \Big[\int_0^{t_1} \big((t_1 - s)^{\alpha-1} - (t_2 - s)^{\alpha-1} \big) \mathrm{d}s + \int_{t_1}^{t_2} (t_2 - s)^{\alpha-1} \mathrm{d}s \Big] \\ &= \frac{M_F}{\Gamma(\alpha+1)} \big[t_1^\alpha - t_2^\alpha + 2(t_2 - t_1)^\alpha \big] \leq \frac{2M_F}{\Gamma(\alpha+1)} (t_2 - t_1)^\alpha,\end{aligned}$$

using $t_2^\alpha \geq t_1^\alpha$. The family $(\boldsymbol{x}^n)$ is thus uniformly bounded and uniformly α-Hölder, hence equicontinuous; by Arzelà–Ascoli a subsequence (not relabelled) converges uniformly on $[0, T]$ to some $\boldsymbol{x}^* \in C([0, T]; \Omega)$. By Step 2 a further subsequence satisfies $\boldsymbol{u}^n \rightharpoonup \boldsymbol{u}^*$ weakly in $(L^2(0, T))^3$ with $\boldsymbol{u}^* \in \mathcal{U}$.

It remains to check that $\boldsymbol{x}^*$ is the state generated by $\boldsymbol{u}^*$. Fix $t \in [0, T]$ and set $K_t(s) = (t - s)^{\alpha-1} \in L^1(0, t)$. The autonomous part passes to the limit by uniform convergence and the Lipschitz continuity of F_0 on Ω. For the control-dependent part we split

$$\int_0^t K_t \big(u_i^n G_i(\boldsymbol{x}^n) - u_i^* G_i(\boldsymbol{x}^*) \big) \mathrm{d}s = \underbrace{\int_0^t K_t \, u_i^n \big(G_i(\boldsymbol{x}^n) - G_i(\boldsymbol{x}^*) \big) \mathrm{d}s}_{(a)} + \underbrace{\int_0^t K_t \big(u_i^n - u_i^* \big) G_i(\boldsymbol{x}^*) \mathrm{d}s}_{(b)} .$$

Term (a) is bounded by $u_i^{\max} \, \|K_t\|_{L^1} \operatorname{Lip}(G_i) \, \|\boldsymbol{x}^n - \boldsymbol{x}^*\|_\infty \to 0$; term (b) tends to 0 because $K_t G_i(\boldsymbol{x}^*)$ is integrable and $u_i^n - u_i^*$ converges weakly to zero. Passing to the limit in the Volterra equation yields $\boldsymbol{x}^*(t) = \boldsymbol{x}_0 + \Gamma(\alpha)^{-1} \displaystyle\int_0^t (t - s)^{\alpha-1} F(s, \boldsymbol{x}^*, \boldsymbol{u}^*) \mathrm{d}s$ for every t, so $(\boldsymbol{x}^*, \boldsymbol{u}^*)$ is admissible.

Finally $\displaystyle\int_0^T (A_1 I^n + A_2 A^n) \mathrm{d}t \to \int_0^T (A_1 I^* + A_2 A^*) \mathrm{d}t$ by uniform convergence, while $\boldsymbol{u} \mapsto \displaystyle\frac{1}{2} \int_0^T \sum_i w_i u_i^2 \mathrm{d}t$ is convex and strongly continuous on $(L^2(0, T))^3$, hence weakly lower semicontinuous. Therefore $J(\boldsymbol{u}^*) \leq \liminf_n J(\boldsymbol{u}^n) = J^* = \inf_{\mathcal{U}} J$, and since $\boldsymbol{u}^* \in \mathcal{U}$ the inequality is an equality. □

Remark 9.3
Strict convexity of L in $\boldsymbol{u}$ gives uniqueness of the optimal control for T small enough, by the standard argument that the state-to-control map is Lipschitz with constant $O(T^\alpha)$; for the twelve-month horizon used in Section 9.1 we claim existence only, and report the control obtained by the sweep as *an* optimal control satisfying the necessary conditions of Theorem 9.4.

Necessary conditions follow from the fractional Pontryagin maximum principle of Agrawal [36] and Kamocki [35]: for a left Caputo state dynamics on $[0, T]$ the co-state solves a *right* Caputo system integrated backwards from a zero terminal condition, the transversality condition $\lambda_i(T) = 0$ expressing that no terminal cost is imposed. Define the Hamiltonian

$$\mathcal{H} = A_1 I + A_2 A + \tfrac{1}{2} \textstyle\sum_i w_i u_i^2 + \lambda_S f_S + \lambda_E f_E + \lambda_I f_I + \lambda_A f_A + \lambda_Q f_Q + \lambda_R f_R, \tag{20}$$

where $f_\bullet$ are the right-hand sides of (16) and $\boldsymbol{\lambda} = (\lambda_S, \ldots, \lambda_R)$ the adjoint variables, $\lambda_j(t)$ being the marginal cost of one additional individual in compartment j at time t.

Because the incidence depends on *all six* state variables through the total population N, its partial derivatives must be computed with care; omitting the N-dependence is the commonest error in this class of models. Put $B := \beta(1-u_1)(I+\eta A)S/N$ and $B_j := \partial B/\partial x_j$, and apply the quotient rule with $\partial N/\partial x_j = 1$ for every j:

$$\begin{aligned}
B_S &= \beta(1-u_1)(I+\eta A)\Big(\frac{1}{N}-\frac{S}{N^2}\Big) = \beta(1-u_1)\frac{(I+\eta A)(N-S)}{N^2},\\
B_I &= \beta(1-u_1)S\Big(\frac{1}{N}-\frac{I+\eta A}{N^2}\Big) = \beta(1-u_1)\frac{S[N-(I+\eta A)]}{N^2},\\
B_A &= \beta(1-u_1)S\Big(\frac{\eta}{N}-\frac{I+\eta A}{N^2}\Big) = \beta(1-u_1)\frac{S[\eta N-(I+\eta A)]}{N^2},\\
B_E &= B_Q = B_R = -\beta(1-u_1)\frac{(I+\eta A)S}{N^2} = -\frac{B}{N},
\end{aligned} \tag{21}$$

the last line because E, Q and R enter B only through the denominator N. The epidemiological reading of $B_E = B_Q = B_R < 0$ is that adding an individual to a non-transmitting compartment dilutes the per-contact probability of meeting an infective and therefore *lowers* the force of infection — a genuine feature of standard incidence that mass-action incidence does not possess. Since ι_E and ι_I are state-independent, they do not appear in any adjoint equation.

Theorem 9.4 (Adjoint system and optimality)
Given $\boldsymbol{u}^*$ and the corresponding state, the adjoint variables satisfy the right-Caputo system with transversality $\lambda_i(T) = 0$,

$$\begin{aligned}
&{}^C_tD^\alpha_T\lambda_S = (\lambda_E-\lambda_S)B_S - \mu\lambda_S,\\
&{}^C_tD^\alpha_T\lambda_E = (\lambda_E-\lambda_S)B_E - k_1\lambda_E + \sigma p\,\lambda_I + \sigma(1-p)\lambda_A,\\
&{}^C_tD^\alpha_T\lambda_I = A_1 + (\lambda_E-\lambda_S)B_I - k_I^u\lambda_I + \big(q_I+\varrho_2u_2^*\big)\lambda_Q + \big(\gamma_I+\varrho_3u_3^*\big)\lambda_R,\\
&{}^C_tD^\alpha_T\lambda_A = A_2 + (\lambda_E-\lambda_S)B_A - k_A\lambda_A + q_A\lambda_Q + \gamma_A\lambda_R,\\
&{}^C_tD^\alpha_T\lambda_Q = (\lambda_E-\lambda_S)B_Q - k_Q\lambda_Q + \gamma_Q\lambda_R, \quad {}^C_tD^\alpha_T\lambda_R = (\lambda_E-\lambda_S)B_R - \mu\lambda_R,
\end{aligned} \tag{22}$$

and the optimal controls are

$$\begin{aligned}
u_1^* &= \min\Big\{u_1^{\max}, \max\Big\{0, \frac{(\lambda_E-\lambda_S)\beta(I+\eta A)S}{w_1N}\Big\}\Big\},\\
u_2^* &= \min\Big\{u_2^{\max}, \max\Big\{0, \frac{\varrho_2(\lambda_I-\lambda_Q)I}{w_2}\Big\}\Big\},\\
u_3^* &= \min\Big\{u_3^{\max}, \max\Big\{0, \frac{\varrho_3(\lambda_I-\lambda_R)I}{w_3}\Big\}\Big\}.
\end{aligned} \tag{23}$$

Proof
The proof has three parts: the co-state equations, their solvability, and the pointwise minimisation.

(a) The adjoint equations. By the fractional maximum principle [35, 36], applicable because F is continuously differentiable in $\boldsymbol{x}$ on the neighbourhood of Ω where $N \geq N_{\min} > 0$ and L is continuously differentiable in $(\boldsymbol{x}, \boldsymbol{u})$, the co-state satisfies ${}^C_tD^\alpha_T\lambda_j = \partial\mathcal{H}/\partial x_j$ with $\lambda_j(T) = 0$. We compute the six partial derivatives of (20) one by one, using (21) and recalling that B appears with a minus sign in f_S and a plus sign in f_E, so that every partial of B enters through the *difference* $\lambda_E - \lambda_S$ — the marginal cost of converting one susceptible into one exposed individual.

For $x_j = S$: only f_S and f_E depend on S, giving $\partial\mathcal{H}/\partial S = \lambda_S(-B_S-\mu) + \lambda_EB_S = (\lambda_E-\lambda_S)B_S - \mu\lambda_S$. For $x_j = E$: f_S and f_E contribute $(\lambda_E-\lambda_S)B_E$, the exit term $-k_1E$ contributes $-k_1\lambda_E$, and E feeds I and A at rates σp and $\sigma(1-p)$, contributing $\sigma p\lambda_I + \sigma(1-p)\lambda_A$; the importation terms contribute nothing, being state-independent. For $x_j = I$: the running cost contributes A_1, the incidence $(\lambda_E-\lambda_S)B_I$, the total controlled removal $-k_I^u\lambda_I$, and the two destinations of removed symptomatic cases $(q_I+\varrho_2u_2^*)\lambda_Q$ and $(\gamma_I+\varrho_3u_3^*)\lambda_R$. The analogous computation for $x_j = A$ gives the fourth line, with A_2 from the running cost. For $x_j = Q$ and $x_j = R$:

these compartments neither transmit nor appear in the running cost, so they influence the dynamics only through the dilution term $B_Q = B_R = -B/N$ and their own exit rates, giving the last two lines. Collecting the six expressions yields (22). The terminal condition $\lambda_j(T) = 0$ holds because (19) contains no terminal payoff.

(b) Solvability of the adjoint system. Along the optimal pair the coefficients B_j are continuous and bounded on $[0, T]$, since $\boldsymbol{x}^* \in C([0, T]; \Omega)$ and $N^* \geq N_{\min} > 0$. System (22) is therefore *linear* in $\boldsymbol{\lambda}$ with bounded continuous coefficients; under the reflection $\tau = T - t$, which maps ${}_t^C D_T^\alpha$ into the left Caputo derivative, it becomes a linear left-Caputo initial-value problem with datum $\boldsymbol{\lambda} = 0$, and Theorem 4.4 applies to give a unique continuous solution on $[0, T]$.

(c) Characterisation of the controls. The maximum principle requires $\mathcal{H}$ to be minimised over $\mathcal{U}$ pointwise a.e. Since $\partial^2 \mathcal{H}/\partial u_i^2 = w_i > 0$ and the mixed second derivatives vanish, $\mathcal{H}$ is strictly convex in $\boldsymbol{u}$, so the unconstrained stationary point is the unique unconstrained minimiser and the constrained minimiser over the box $\prod_i [0, u_i^{\max}]$ is its componentwise projection. Setting $\partial \mathcal{H}/\partial u_i = 0$ and using $\partial B/\partial u_1 = -\beta(I + \eta A)S/N$,

$$\frac{\partial \mathcal{H}}{\partial u_1} = w_1 u_1 - (\lambda_E - \lambda_S)\frac{\beta(I + \eta A)S}{N} = 0$$

$$\frac{\partial \mathcal{H}}{\partial u_2} = w_2 u_2 - \varrho_2 I(\lambda_I - \lambda_Q) = 0,$$

$$\frac{\partial \mathcal{H}}{\partial u_3} = w_3 u_3 - \varrho_3 I(\lambda_I - \lambda_R) = 0,$$

whence the three stationary values, whose projection onto $[0, u_i^{\max}]$ gives (23).

The characterisation is epidemiologically transparent. Effort is applied in proportion to the marginal benefit it buys and inversely to its unit cost: u_1 is driven by the marginal cost of a new infection, $\lambda_E - \lambda_S$, multiplied by the number of infections currently being generated per unit time; u_2 by the gain from moving a symptomatic case into isolation, $\lambda_I - \lambda_Q$; and u_3 by the gain from moving one into recovery, $\lambda_I - \lambda_R$. Whenever a marginal gain is non-positive the projection sets the corresponding effort to zero, and whenever it is large the effort saturates at its upper bound. □

9.1. Numerical results

The optimality system (16), (22), (23) is a two-point boundary-value problem — the state is given at $t = 0$, the co-state at $t = T$ — and is solved by the forward–backward sweep. Starting from $\boldsymbol{u}^{(0)} \equiv 0$, each iteration k performs three operations: the state is integrated forward on a uniform grid $t_n = nh$ with the $L1$ discretisation of the left Caputo derivative; the adjoint is integrated backward from $\boldsymbol{\lambda}(T) = 0$ after the reflection $\tau = T - t$, which converts the right-Caputo operator into a left-Caputo one so that the same $L1$ scheme applies; and the controls are updated by (23) under damped relaxation

$$\boldsymbol{u}^{(k+1)} = \omega\, \widehat{\boldsymbol{u}}^{(k)} + (1 - \omega)\, \boldsymbol{u}^{(k)}, \quad \omega = 0.4, \tag{24}$$

where $\widehat{\boldsymbol{u}}^{(k)}$ is the raw characterisation evaluated at the current state and co-state. Damping is necessary: the undamped map oscillates, because u_1 enters the incidence multiplicatively while the co-state responds to the state with the opposite time orientation. The sweep terminates when the increments of the three control families, measured in the supremum norm on $[0, T]$, fall below a common tolerance,

$$\sum_{i=1}^{3} \left\| u_i^{(k)} - u_i^{(k-1)} \right\|_\infty < \epsilon = 10^{-3}. \tag{25}$$

Using the importation-augmented baseline ($\alpha = 0.90$, $T = 12$ months, $h = 0.1$, and the control parameters of Table 5), the sweep meets (25) in 16 iterations. Figure 11 shows that the optimal strategy cuts the symptomatic peak by about 76% (from ≈ 61 to ≈ 15) and the total infected burden $\int_0^T (I+A)\mathrm{d}t$ by about 75%. Figure 12 shows the optimal profiles: after a brief initial transient in which it saturates at its upper bound, contact reduction u_1 falls back, then rises again through the importation surge and is relaxed afterwards, while isolation u_2 and treatment u_3 track symptomatic prevalence. Thus, even for an importation-sustained outbreak with endogenous $\mathcal{R}_0 < 1$, coordinated control substantially reduces the burden generated by importation.

It is natural to ask how much of this gain is specific to the sub-critical, importation-driven regime, and Reviewer feedback prompted us to quantify it. We therefore repeated the entire exercise on a hypothetical variant in which the transmission rate alone is raised until the endogenous reproduction number becomes super-critical, $\mathcal{R}_0 = 1.50$ (that is, $\beta = 5.811$ against the fitted 3.632), every other parameter, the importation pulse and the control weights being held fixed. Without control the two regimes are not comparable in magnitude: the symptomatic peak rises from 60.6 to 9140.9 and the burden from 423.8 to 5.55×10^4 person-months, because local transmission now sustains itself instead of decaying between importation events. Under the optimal control, however, the two regimes end in almost the same place: the peak is 13.50 against 14.50 and the burden 108.1 against 107.8 person-months, so the relative reduction is 99.8% in the super-critical regime against about 75% in the calibrated one. (The super-critical sweep requires the relaxation weight to be reduced to $\omega = 0.2$, at which it converges in 30 iterations; at $\omega = 0.4$ the iteration oscillates without meeting (25).)

The comparison is informative in two ways. It shows, first, that the $\approx 75\%$ figure reported above is a *conservative* measure of what the strategy achieves, because in the sub-critical regime much of the burden is imported and is by construction beyond the reach of the three interventions, which act on local transmission, isolation and recovery but not on the border. Second, it shows that the optimal strategy is not merely trimming a decaying transient: confronted with a genuinely self-propagating epidemic it suppresses the wave almost entirely, at the cost of holding u_1 at its upper bound $u_1^{\max} = 0.80$ for a substantially longer interval. The practical reading for the 2024 Algerian outbreak is that the modest headroom left by $\mathcal{R}_0 < 1$ makes border surveillance, rather than intensified local control, the binding intervention — which is the same conclusion reached from the calibration in Section 7.

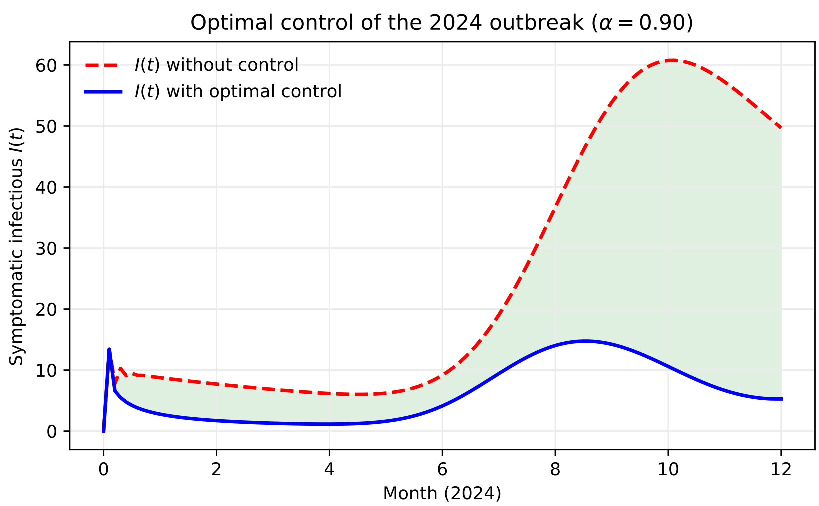

Figure 11. Symptomatic infectious $I(t)$ without control (dashed) and under the optimal control (solid); the shaded area is the averted burden.

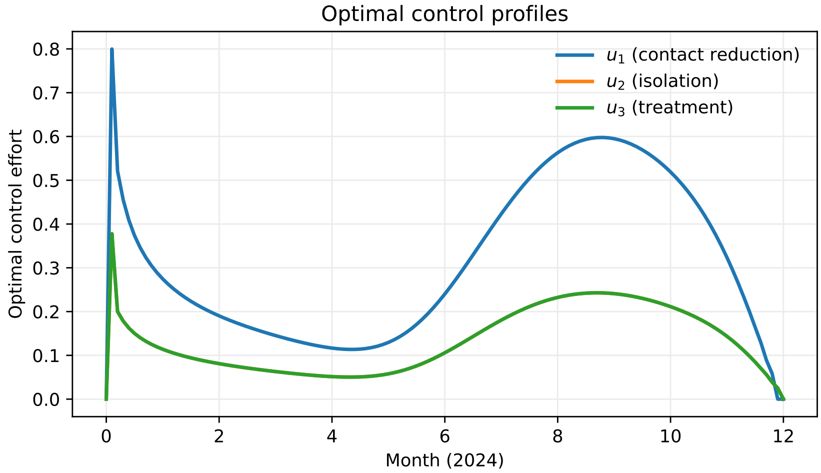

Figure 12. Optimal control profiles u_1 (contact reduction), u_2 (isolation) and u_3 (treatment) over the 2024 outbreak window. The u_2 and u_3 profiles coincide to plotting accuracy, the orange curve lying beneath the green one: with $\varrho_2 = \varrho_3$ and $w_2 = w_3$ the two characterisations in (23) differ only through λ_Q versus λ_R, and the Q and R adjoints track each other closely because neither compartment transmits nor enters the running cost (19).

10. Conclusion

We analysed a six-compartment $SEIAQR$ model under the Caputo and Atangana–Baleanu–Caputo operators, proving positive invariance and ultimate boundedness in $\mathbb{R}_+^6$ via a fractional comparison theorem and well-posedness via the Banach fixed-point theorem for both operators. The basic reproduction number (8) was obtained in closed form and shown to be order-independent; the disease-free equilibrium is locally (Matignon, Routh–Hurwitz) and globally (Goh-type Lyapunov, fractional LaSalle) stable when $\mathcal{R}_0 \le 1$, and a unique endemic equilibrium is globally stable for $\mathcal{R}_0 > 1$ under a Goh–Volterra condition. Closed-form sensitivity indices identified the transmission rate and the symptomatic recovery rate as the dominant controls.

Applying the model to the 2024 diphtheria outbreak in Algeria with national INSP surveillance data, and making the cross-border importation explicit through a time-varying term $\iota(t)$, we reduced the calibration error by about 30% over the autonomous model and obtained the key finding that the endogenous reproduction number is $\mathcal{R}_0 \approx 0.93 < 1$: the outbreak was *importation-sustained* rather than self-propagating, a conclusion coherent with the global stability of the disease-free state and consistent with Algeria's high vaccination coverage. The memory order plays a secondary role for this short-course disease — it governs the transient shape but the fast autumn decline favours near-exponential ($\alpha \to 1$) relaxation. Finally, a fractional optimal-control analysis (existence, Caputo adjoints, Pontryagin characterization) showed that a coordinated contact-reduction, isolation and treatment strategy cuts the infected burden by about 75%, so that even an importation-sustained outbreak is strongly controllable. Open directions include stochastic and variable-order extensions and a cost-effectiveness analysis of the individual interventions.

The last of these changes the class of the optimisation problem rather than merely extending it. Section 9 minimises an additive cost (19) over a fixed horizon; a health authority instead faces the dual question of which mix of interventions maximises the burden averted *per unit spent* under a fixed budget. That objective is a ratio of two linear functionals of the intervention levels over a polytope defined by the budget and the bounds $0 \le u_i \le u_i^{\max}$, hence a linear fractional programme, of moderate dimension and with bounded variables — the setting of the hybrid direction method of Hakmi *et al.* [37]. We note that "fractional" there refers to the ratio structure of the objective and not to the memory order α, so the two senses of the word are unrelated.

Acknowledgement

The authors thank the Institut National de Santé Publique (Algeria) for making the national epidemiological bulletins publicly available.

REFERENCES

1. W. O. Kermack, and A. G. McKendrick, *A contribution to the mathematical theory of epidemics*, Proceedings of the Royal Society A, vol. 115, pp. 700–721, 1927.
2. I. Podlubny, *Fractional Differential Equations*, Academic Press, San Diego, 1999.
3. A. A. Kilbas, H. M. Srivastava, and J. J. Trujillo, *Theory and Applications of Fractional Differential Equations*, Elsevier, Amsterdam, 2006.
4. K. Diethelm, *The Analysis of Fractional Differential Equations*, Lecture Notes in Mathematics, vol. 2004, Springer, Berlin, 2010.
5. M. Caputo, *Linear models of dissipation whose Q is almost frequency independent – II*, Geophysical Journal International, vol. 13, no. 5, pp. 529–539, 1967.
6. K. S. Miller, and B. Ross, *An Introduction to the Fractional Calculus and Fractional Differential Equations*, John Wiley & Sons, New York, 1993.
7. A. Atangana, and D. Baleanu, *New fractional derivatives with nonlocal and non-singular kernel: theory and application to heat transfer model*, Thermal Science, vol. 20, no. 2, pp. 763–769, 2016.
8. M. Caputo, and M. Fabrizio, *A new definition of fractional derivative without singular kernel*, Progress in Fractional Differentiation and Applications, vol. 1, no. 2, pp. 73–85, 2015.
9. J. Losada, and J. J. Nieto, *Properties of a new fractional derivative without singular kernel*, Progress in Fractional Differentiation and Applications, vol. 1, no. 2, pp. 87–92, 2015.
10. M. Toufik, and A. Atangana, *New numerical approximation of fractional derivative with non-local and non-singular kernel: application to chaotic models*, The European Physical Journal Plus, vol. 132, art. 444, 2017.
11. S. Ullah, M. A. Khan, and M. Farooq, *A new fractional model for tuberculosis with relapse via Atangana–Baleanu derivative*, Chaos, Solitons & Fractals, vol. 116, pp. 63–71, 2018.
12. M. A. Khan, and A. Atangana, *Modeling the dynamics of novel coronavirus (2019-nCov) with fractional derivative*, Alexandria Engineering Journal, vol. 59, no. 4, pp. 2379–2389, 2020.
13. E. Ahmed, A. M. A. El-Sayed, and H. A. A. El-Saka, *Equilibrium points, stability and numerical solutions of fractional-order predator–prey and rabies models*, Journal of Mathematical Analysis and Applications, vol. 325, no. 1, pp. 542–553, 2007.
14. M. Tafrikan, Fatmawati, Windarto, and C. E. Madubueze, *Fractional dynamics and sensitivity analysis of a diphtheria spread model*, Statistics, Optimization & Information Computing, vol. 16, no. 3, pp. 1884–1914, 2026.
15. S. N. Afiyah, Fatmawati, Windarto, and A. Abidemi, *Dynamics of a fractional order harvested predator–prey model incorporating fear effect and refuge*, Statistics, Optimization & Information Computing, vol. 13, no. 4, pp. 1690–1713, 2025.
16. F. F. Herdicho, Fatmawati, C. Alfiniyah, and C. W. Chukwu, *Hybrid Euler method and Pontryagin principle in fractional dengue model with sex classification and optimal controls*, Statistics, Optimization & Information Computing, vol. 14, no. 1, 2025.
17. M. A. Hidayat, Fatmawati, C. Alfiniyah, and E. Bonyah, *Optimal control strategy for fractional model of monkeypox transmission under real data*, Statistics, Optimization & Information Computing, vol. 15, pp. 3761–3779, 2026.
18. M. A. Hidayat, Fatmawati, C. Alfiniyah, and O. J. Peter, *A time-delayed mathematical modeling for monkeypox transmission with incubation period*, Statistics, Optimization & Information Computing, vol. 14, no. 6, pp. 3874–3890, 2025.
19. C. Alfiniyah, F. Putri Batubara, Ahmadin, and R. Gweryina, *Modeling and optimal control analysis of Lassa fever with lockdown and treatment interventions*, Statistics, Optimization & Information Computing, vol. 16, no. 2, pp. 1243–1254, 2026.
20. Institut National de Santé Publique (Algérie), *Relevé Épidémiologique Mensuel (R.E.M.), situation épidémiologique de l'année 2024*, Vol. XXXV, INSP, Alger, 2025. Available: https://www.insp.dz.
21. World Health Organization, *Diphtheria reported cases and incidence* (WHO/UNICEF Joint Reporting Form on Immunization), WHO Immunization Data portal, 2026. Available: https://immunizationdata.who.int.
22. N. Aguila-Camacho, M. A. Duarte-Mermoud, and J. A. Gallegos, *Lyapunov functions for fractional order systems*, Communications in Nonlinear Science and Numerical Simulation, vol. 19, no. 9, pp. 2951–2957, 2014.
23. C. Vargas-De-León, *Volterra-type Lyapunov functions for fractional-order epidemic systems*, Communications in Nonlinear Science and Numerical Simulation, vol. 24, pp. 75–85, 2015.
24. D. Matignon, *Stability results for fractional differential equations with applications to control processing*, in Computational Engineering in Systems Applications, vol. 2, pp. 963–968, 1996.
25. Y. Li, Y. Chen, and I. Podlubny, *Mittag–Leffler stability of fractional order nonlinear dynamic systems*, Automatica, vol. 45, no. 8, pp. 1965–1969, 2009.
26. H. Delavari, D. Baleanu, and J. Sadati, *Stability analysis of Caputo fractional-order nonlinear systems revisited*, Nonlinear Dynamics, vol. 67, pp. 2433–2439, 2012.
27. J. Huo, H. Zhao, and L. Zhu, *The effect of vaccines on backward bifurcation in a fractional order HIV model*, Nonlinear Analysis: Real World Applications, vol. 26, pp. 289–305, 2015.
28. P. van den Driessche, and J. Watmough, *Reproduction numbers and sub-threshold endemic equilibria for compartmental models of disease transmission*, Mathematical Biosciences, vol. 180, pp. 29–48, 2002.
29. O. Diekmann, J. A. P. Heesterbeek, and J. A. J. Metz, *On the definition and the computation of the basic reproduction ratio R_0 in models for infectious diseases in heterogeneous populations*, Journal of Mathematical Biology, vol. 28, pp. 365–382, 1990.
30. N. Chitnis, J. M. Hyman, and J. M. Cushing, *Determining important parameters in the spread of malaria through the sensitivity analysis of a mathematical model*, Bulletin of Mathematical Biology, vol. 70, pp. 1272–1296, 2008.

31. K. Diethelm, N. J. Ford, and A. D. Freed, *A predictor–corrector approach for the numerical solution of fractional differential equations*, Nonlinear Dynamics, vol. 29, pp. 3–22, 2002.
32. R. Garrappa, *Numerical solution of fractional differential equations: a survey and a software tutorial*, Mathematics, vol. 6, no. 2, art. 16, 2018.
33. Z. Odibat, and S. Momani, *An algorithm for the numerical solution of differential equations of fractional order*, Journal of Applied Mathematics & Informatics, vol. 26, pp. 15–27, 2008.
34. W. H. Fleming, and R. W. Rishel, *Deterministic and Stochastic Optimal Control*, Springer-Verlag, New York, 1975.
35. R. Kamocki, *Pontryagin maximum principle for fractional ordinary optimal control problems*, Mathematical Methods in the Applied Sciences, vol. 37, no. 11, pp. 1668–1686, 2014.
36. O. P. Agrawal, *A general formulation and solution scheme for fractional optimal control problems*, Nonlinear Dynamics, vol. 38, pp. 323–337, 2004.
37. M. A. Hakmi, M. Bentobache, and M. O. Bibi, *A hybrid direction method for linear fractional programming*, Statistics, Optimization & Information Computing, vol. 13, pp. 922–948, 2025.